1979

Propagation of flexure cracks in glass and polymethylmethacrylate plates

Yung-Tze Henry Chen
Iowa State University

CHEN, YUNG-TZE HENRY

PROPAGATION OF FLEXURE CRACKS IN GLASS AND POLYMETHYLMETHACRYLATE PLATES

Iowa State University PH.D. 1979

PLEASE NOTE:

In all cases this material has been filmed in the best possible way from the available copy. Problems encountered with this document have been identified here with a check mark ✓.

1. Glossy photographs _____
2. Colored illustrations _____
3. Photographs with dark background ✓
4. Illustrations are poor copy _____
5. Print shows through as there is text on both sides of page _____
6. Indistinct, broken or small print on several pages _____ throughout _____
7. Tightly bound copy with print lost in spine _____
8. Computer printout pages with indistinct print _____
9. Page(s) _____ lacking when material received, and not available from school or author _____
10. Page(s) _____ seem to be missing in numbering only as text follows _____
11. Poor carbon copy _____
12. Not original copy, several pages with blurred type _____
13. Appendix pages are poor copy _____
14. Original copy with light type _____
15. Curling and wrinkled pages _____
16. Other _____

University Microfilms International

300 N. ZEEB RD., ANN ARBOR, MI 48106 (313) 761-4700

Propagation of flexure cracks in glass and polymethylmethacrylate plates

by

Yung-Tze Henry Chen

A Dissertation Submitted to the
Graduate Faculty in Partial Fulfillment of the
Requirement for the Degree of
DOCTOR OF PHILOSOPHY

Department: Engineering Science and Mechanics
Major: Engineering Mechanics

Approved:

Signature was redacted for privacy.

In Charge of Major Work

Signature was redacted for privacy.

For the Major Department

Signature was redacted for privacy.

For the Graduate College

Iowa State University
Ames, Iowa

1979

TABLE OF CONTENTS

		Page
I.	INTRODUCTION	1
II.	LITERATURE REVIEW	3
III.	PROPAGATION OF FLEXURE CRACK IN GLASS PLATES	10
	A. Experiment	10
	1. Experimental set-up	10
	2. Experimental procedure	12
	B. Analysis	14
	C. Results	27
IV.	PROPAGATION AND SURFACE ENERGY OF FLEXURE CRACK IN POLYMETHYLMETHACRYLATE PLATES	34
	A. Crack Propagation	34
	1. Measurement of crack speed	34
	2. Results	36
	B. Surface Energy	40
	1. Quasi-static surface energy	40
	a. Experimental set-up and procedure	40
	b. Results	42
	2. Dynamic surface energy	44
	a. Experimental set-up and procedure	44
	b. Results	48
V.	HERTZIAN FRACTURE AND FLEXURE FRACTURE PRODUCED BY IMPACT IN GLASS PLATES	55
	A. Experimental Set-Up and Procedure	55
	B. Results	57
VI.	CONCLUSION AND SUMMARY	62
VII.	BIBLIOGRAPHY	65

		Page
VIII.	ACKNOWLEDGEMENTS	68
IX.	APPENDIX A. CALCULATION OF a, V, δ AND f	69
	A. Case 1 - Unfractured PMMA Plate	69
	B. Case 2 - Fractured PMMA Plate	71
X.	APPENDIX B. CALCULATION OF SURFACE ENERGY	76
	A. Case 1 - Quasi-Static Loading	76
	B. Case 2 - Impact Loading	77
XI.	APPENDIX C. DESCRIPTION OF IMPACT THEORY	79

I. INTRODUCTION

The work presented in the dissertation is concerned with the propagation of flexure cracks in glass and polymethylmethacrylate (PMMA) plates which are subjected to transverse static or dynamic loadings. The loading is applied to a surface of a glass or PMMA plate specimen whereas the other surface of the specimen is supported by a foundation of various spans. The plate specimens are loaded until fracture occurs. In most of the cases studied, the span of the support is comparable to the plate thickness and therefore a three-dimensional stress field is produced in the specimen. The work presented falls into three parts; namely, 1) propagation of flexure crack in glass plates, 2) propagation and surface energy of flexure crack in PMMA plates, and 3) Hertzian fracture and flexure fracture produced by impact in glass plates.

In the first study, a fracture propagating in a glass plate subjected to a transverse static load is produced and the varying speed of the propagating flexure crack is measured experimentally. In addition, an analysis of the three-dimensional state of stresses in the specimens is described and factors controlling the process of fracturing are examined in terms of the analytical results obtained.

The second study is concerned with fractures produced in PMMA plate specimens. The crack speed of a flexure crack

running in a PMMA plate is measured experimentally, and is compared to that for a glass plate. The surface energy of a PMMA plate specimen under a transverse quasi-static or dynamic loading is also determined.

Fracture produced by impinging a steel ball onto a surface of a glass plate specimen is investigated in the third study. The glass plate is supported by a foundation on its other unloaded surface. The ratio of the plate thickness to the span of the foundation is chosen to be in the range where the three-dimensional stress effects are important. As a result, two types of fractures, Hertzian fractures and flexure fracture are produced in the glass plate specimens. The dynamic fracture strength and the condition for transition from one type of fracture to the other are investigated by varying the size of the support span.

II. LITERATURE REVIEW

Fracture velocities in glasses have been measured by the techniques of high-speed photography (1). It was observed that if a fracture propagates, it travels with a maximum constant speed of 1500 m/sec. Using the methods of an electrically conductive grid, measurements were made on the speed of a crack propagation in a glass plate under a constant bending moment (2). For a given state of loading, the crack speed was measured to be constant. However, the crack speed varied from 215 m/sec to 1520 m/sec, depending upon the state of loading. Indeed, the crack speed was shown to be dependent upon the magnitude of stress (2). The stress waves generated by the fracture of glass beams of a rectangular cross-section subjected to pure bending were recorded recently by using the strain gage techniques (3). It was observed that both longitudinal and bending waves were emitted during the fracture process.

Study on the behavior of polymers was made at the U.S. Naval Research Laboratories (4), after a number of unexpected catastrophic failures of aircraft cockpit canopies which were fabricated from moulded Lucite (an American tradename for PMMA) occurred under combat conditions. Under high strain-rate conditions, as happens in the case of a running unstable crack, PMMA behaves as a close approximation to an ideally brittle material.

Hence its fracture behavior may be well described by the theory of linear elastic fracture mechanics. However, PMMA is a viscoelastic material, and its material properties were expected to be time-dependent at low strain rate (5). Furthermore, at very high strain rate of loading, the modulus of PMMA increases very quickly with increasing strain rate (6). To investigate the rapid fracture behavior of PMMA by linear fracture mechanics, some knowledge of the appropriate material parameters is required as pointed out by Cotterell (7). A series of crack speed measurements was performed on wedge-loaded double-cantilever-beam specimens of commercial PMMA. Anthony's method was used for measuring crack velocity (8). Among the complexities observed in the experiments that need explanation is the great variability in crack speed. For example, in the work of Watts and Burns on PMMA (9), a change of stress intensity of less than a factor of two, was accompanied by a change in crack speed of well over three orders of magnitude. Berry (10) reported a difference in speed between slow and fast crack growth of five orders of magnitude. These changes are reflected in a variety of velocity-dependent fracture surface markings (11).

An explanation of brittle strength phenomena was first proposed by Griffith (12) in 1920, partly based on the earlier work of Inglis (13), who analyzed the elastic stress distribution around an elliptical hole in a stressed plate, utilizing

the classical method of elasticity. Griffith assumed that the discrepancy between theoretically estimated and experimentally observed values of tensile strength was due to the presence of very small cracks or flaws around which a stress concentration arose when the solid was loaded. He made use of Inglis's calculation by regarding these cracks as very flat elliptical holes, and postulated that the crack would lengthen and cause fracture if, for a small increase of its length, the release in elastic strain energy became equal to the energy required to form new surfaces. The analysis leads to Griffith's well known expression:

$$\sigma = (2\gamma E/\pi C)^{\frac{1}{2}}$$

where σ is tensile strength, γ is surface energy, E is Young's modulus, and 2C is the length of a surface crack. The equation requires the condition that the thickness of the plate is small compared to the crack length, or more precisely, that a state of plane stress prevails. For a thick plate under a state of plane strain, the equation is modified as

$$\sigma = [2E\gamma/C(1 - \nu^2)]^{\frac{1}{2}}$$

where ν is Poisson's ratio of the material. Griffith verified his theory by producing microscopic flaws in glass tubes which were subsequently burst with internal pressure.

Orowan (14) and Irwin (15) later applied the Griffith criterion to brittle fracture of ship steel. Orowan measured the Griffith surface energy by inserting fine cracks into the solid body and measuring the resulting tensile strength as a function of flaw size. The surface energy so found was 10^6 erg/cm^2, which compares to a theoretical estimate of 10^3 erg/cm^2 on the basis of the reversible work necessary to separate two atomic planes of the metal. This large discrepancy is attributed to the formation of a plastically deformed layer of material near the crack tip. In order to account for this factor, Griffith's equation is modified as

$$\sigma = [2E(\gamma + p)/\pi C]^{\frac{1}{2}}$$

where p is the work of plastic deformation. Orowan (14) showed by means of X-ray diffraction studies that $p >> \gamma$, Irwin (15) employed a centrally notched sheet specimen of metal to determine a quantity, G_c, the critical strain energy release rate. This is equal to 2γ in Griffith's equation and is measured at the instant when a stable crack growing from the notch becomes unstable, propagates rapidly, and causes fracture of the sheet. Because of the additional work required to propagate a crack, it would be more appropriate to name this quantity "fracture surface work."

The Griffith's theory has also been recently applied to polymers by Berry (16). By measuring the tensile strength of

Polystyrene and Polymethylmethacrylate as a function of flaw size, Berry found that the polymers obey Griffith's criterion, and that the tensile strength varies inversely proportional to the square root of the crack length. The fracture surface work for Plexiglas was found to be 3×10^5 erg/cm^2 and the value for Polystyrene was 1.7×10^6 erg/cm^2. The theoretical value for surface energy for glassy polymers was calculated to be 450 erg/cm^2. This large discrepancy between the measured and calculated value is similar to the difference observed for ship steel (inorganic glass does not exhibit this discrepancy). Berry proposed that this high value of the measured surface work was caused by viscous flow at the tip of the crack which results in polymer reorientation. This reorientation hypothesis was based on the prior observations that fresh fracture surface of Plexiglas exhibits bright colors.

The cleavage method was used by Obreimoff (17) for the determination of the surface energy of mica. Later Gilman (18) developed the experimental technique in such a way that the surface energies of simple crystal like Zn could also be measured. A similar method was employed by Brace and Walsh (19) on quartz by Westwood and Hitch (20) on KCl and by Gutshall and Gross (21) on NaCl. PMMA is a popular material for fracture investigation because it is cheap, easy to machine, transparent, and relatively brittle. Recently, Knauss (22) presented a review of the mechanics of fracture in polymers with 221

references. Kambour (23) did some of the definitive work on the surface fracture pattern on PMMA. The response of brittle solids to the impact by steel balls has been investigated by a number of works (24, 25). Andrews (24) and Tillet (25) established that for a sphere of given diameter there existed a critical velocity or drop height to nucleate a cone crack in a given glass. Roesler (26) showed that this observation was simply a restatement of the fact that under quasi-static conditions the critical load to initiate a cone crack was proportional to the indenter radius, so-called Auerbach's law. However, for velocities greatly in excess of the velocity to initiate cone cracks, crushing and the formation of a variety of other cracking systems occurs. These types of cracks were described by Tsai and Kolsky (27), Cherepanov and Sokolinsky (28), primarily from post-impact macroscopic examinations. Works on indentation fracture by Lawn and Swain (29), and Swain and Hagan (30) described the importance of observing the fracturing process during loading and unloading of the indenter. The separate stages of the fracture process were identified and related the state of loading and stress field at a particular time. Lee and Rodak (31) studied analytically the indentation problem for a rigid, spherical indenter and a viscoelastic half space. Hunter (32) obtained coupled integrodifferential equations for the associated impact problem. These equations can be simplified if the area of contact in the

viscoelastic problem is assumed to be different only slightly from that in the associated elastic (Hertz) problem. Vincent (33) and Buchnall et al. (34), gave a general survey of the impact testing of polymers.

III. PROPAGATION OF FLEXURE CRACK IN GLASS PLATES

A. Experiment

The experiment was concerned with the observation of a flexure crack running through the center lines of glass specimens which rested on top of a ring or double knife-edged foundation and designed to measure the crack speed in glass plates under transverse loads.

1. Experimental set-up

The experimental set-up of a double knife-edged foundation is shown in Fig. 1a, and the electrical circuitry for measuring crack speeds is shown in Fig. 1c. A hydraulic press was used for this test. A steel ball of 1 $\frac{3}{4}$" diameter was connected to an adapter (see Fig. 1a) which screwed into the top plate of the hydraulic press. Specimens of glass plates 1/8" x 7" x 3", were used for testing. The spans 2L of the double knife-edge foundation used in the tests were 1/4", 1/2" and 1". Another type of foundation, ring foundation shown in Fig. 1b, was also used in the tests. This type of arrangement is essentially the same as that shown in Fig. 1a, except that the two parallel knife edges are replaced by a circular ridge of diameter 2ρ as was used in (35). The diameters 2ρ used were also 1/4", 1/2" and 1". A six volt Eveready D.C. battery was used as the energy source in the electrical circuitry. A

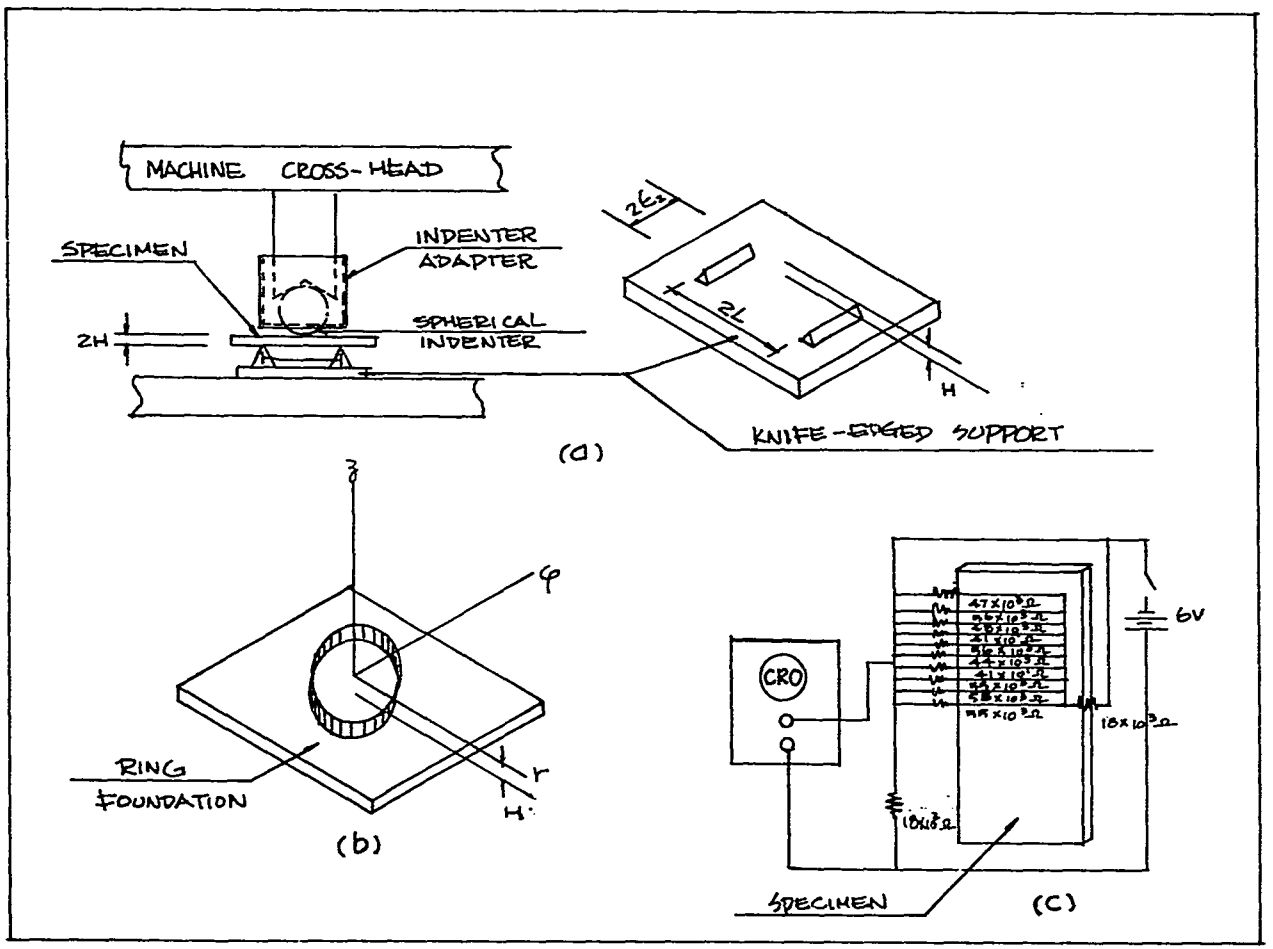

Fig. 1. Experimental set-up for measurement of crack speed

Tektronic 502A dual beam oscilloscope with a Tektronic C-12 camera was used to record the electrical signals generated from the circuitry of Fig. 1b. All external cables were shielded and grounded.

2. Experimental procedure

All the specimens were cut from 1/8" thick glass plates. The specimens of glass plate were all 17.78 x 7.62 x 0.3175 cm. A scratch was introduced starting at about 5 cm from the edge along the center line in the direction of the length on the lower plate surface. Acetone was used to clean the surface of the glass plate. In front of the scratch, 10 silver lines (2" long, 1/4" side, 450 Å thick) of 6.35 mm (center to center) apart were deposited using a vacuum evaporator. The lines were perpendicular to the direction of the scratch, which is the expected direction of fracture. At each end of the silver film grid an electrical terminal was mounted with 5 minute epoxy Eleven electrical wires were used to connect the electrical terminals to a control box which contained the remaining parts necessary for the completion of the circuitry in Fig. 1c. On its upper surface, the plate specimen was loaded with a steel ball of 4.445 cm diameter which was held by an adapter mounted to the machine cross-head of a hydraulic press. The specimen was placed on the upper ends of two parallel triangular edges with ridge radius of 0.4 mm, machined from a steel plate

hardened through heat treatment (see Fig. 1a). The knife edges are all 6.35 mm long, but were made with different spans of 2L. The lower surface of the double knife-edged foundation was placed on the hydraulic press. The center of the contact area between the specimen and the spherical indenter was aligned to coincide with the center of the two knife edges. If the knife-edged foundation is replaced by a ring foundation with diameter of 2ρ, the set-up is called the ring foundation arrangement. During the loading, the center of the contact area was aligned to coincide with the center of the circular support. In order to control the direction of fracture, a scratch was introduced starting at about 5 cm from the edge along the center line in the direction of the length on the lower plate surface. The load was applied on the upper surface opposite the scratch. When fracture occurred, the passage of the crack broke the silver lines in front of the scratch. This generated voltage signals which were fed to a cathode-ray oscilloscope. The trace on the screen of the oscilloscope was photographed, giving the time required for the crack to move from one line to antoher. From this, the velocity of the crack was found as a function of distance from the crack center. The photographs obtained are shown in Fig. 2 for different spans and supports.

B. Analysis

In order to interpret the experimental results obtained, the stress distribution in the specimen is required. Two types of three-dimensional stress field are established in glass plates used in the experiments, depending upon support conditions. The stress field in the plate supported by the ring foundation can be obtained from an earlier work (35) and will be described later. Solutions for the stress field in an infinite elastic plate with thickness 2H supported by the double knife-edged foundation are to be described first. Since the stresses of interest are away from the contact areas of the indenter and the knife edges, the loads produced by the indenter and the knife edges are respectively considered as a concentrated load and line loads of finite length $2\varepsilon_2$ and of span 2L (Fig. 1a). The boundary conditions can be written as the sum of the symmetrical (stretching) and antisymmetrical (bending) component (35). In terms of the coordinates in Fig. 3, the symmetrical components of the normal stresses on the plate surfaces can be written as

$$\sigma_{zz}^{I} = -P\delta(x)\delta(y)/2 - PQ \quad \text{at } z = \pm H \tag{1}$$

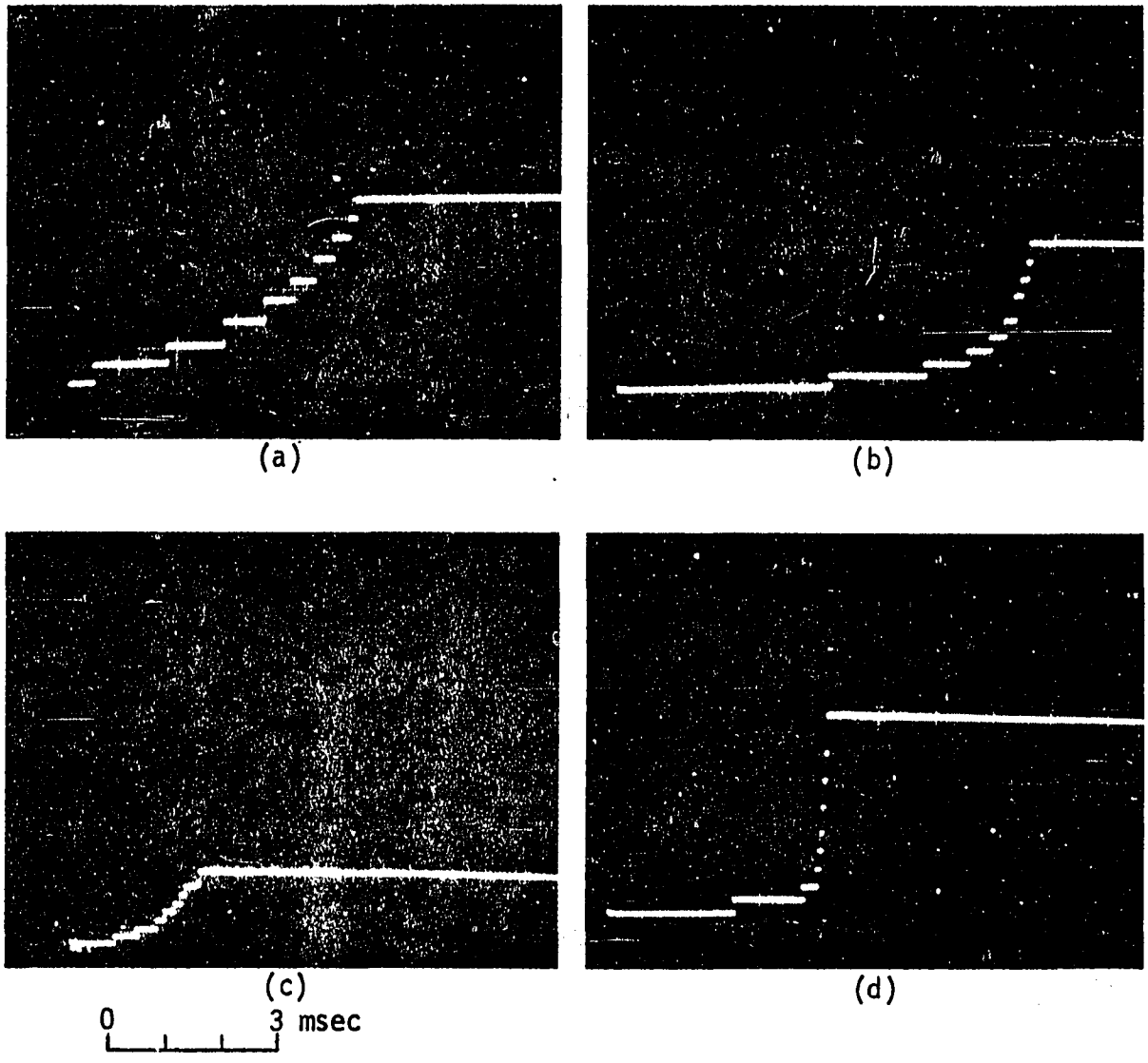

Fig. 2. Oscilloscope trace measuring the flexure crack speed

(a) $2L = 2.54$ cm
(b) $2L = 0.635$ cm
(c) $2\rho = 2.54$ cm
(d) $2\rho = 0.635$ cm

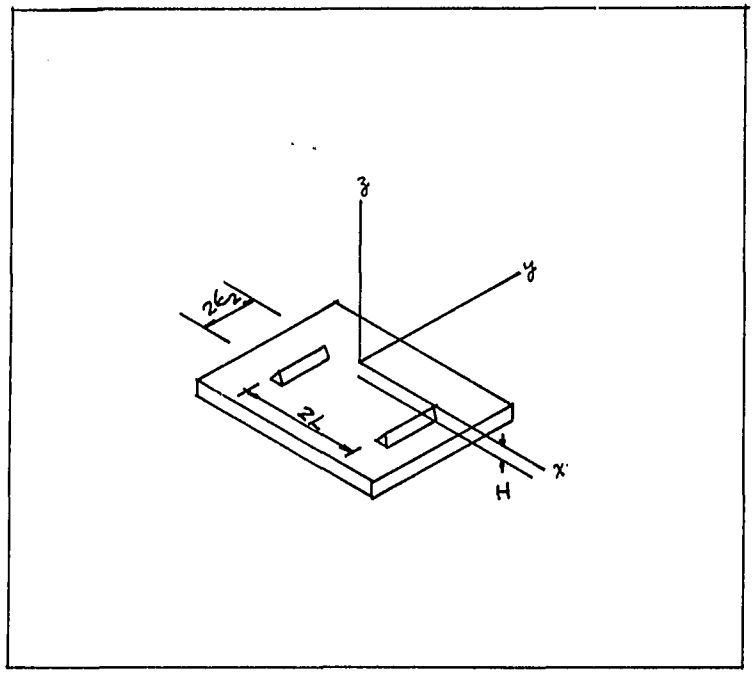

Fig. 3. Coordinate system

where

$$Q = [H(y + \varepsilon_2) - H(y - \varepsilon_2)][\delta(x + L) + \delta(x - L)]/8\varepsilon_2 \quad (2)$$

P is the total load exerted by the indenter on the upper surface. $\delta(x)$ is the delta function, while $H(y)$ is the Heaviside step function. Similarly, the antisymmetrical components of the normal surface stresses are written as

$$\sigma_{zz}^{II} = \mp P\delta(x)\delta(y)/2 \pm PQ \qquad \text{at } z = \pm H \quad (3)$$

The surfaces of the plate are assumed to be smooth so that the shearing stresses σ_{zx} and σ_{zy} on the surface $z = \pm H$ are vanishing. Solutions for the above problem can be constructed through the Fourier cosine integral from the following symmetrical and antisymmetrical basic problems of an infinite elastic plate of thickness 2H. The symmetrical basic problems satisfy the boundary conditions as follows:

$$\bar{\sigma}_{zz}^{I} = D^{I}\cos\xi x\cos\eta y \qquad \text{at } z = \pm H \quad (4)$$

and

$$\bar{\sigma}_{zx}^{I} = \bar{\sigma}_{zy}^{I} = 0 \quad \text{at } z = \pm H \quad (5)$$

where D^{I}, ξ and η are arbitrary constants or parameters which are to be specified in constructing the solutions through the Fourier cosine integrals.

The method of Love's strain function (36) can be used to solve the basic problems. To satisfy the three-dimensional equilibrium equations and the boundary conditions of Equations 4 and 5, the symmetrical Love's strain functions are chosen as follows:

$$Z^I = A^I\psi_2 + B^ICz\psi_1 \tag{6}$$

where

$$\psi_1 = \cos\xi x\cos\eta y\cosh Cz \tag{7}$$

$$\psi_2 = \cos\xi x\cos\eta y\sinh Cz \tag{8}$$

and

$$C^2 = \xi^2 + \eta^2 \tag{9}$$

ψ_1 and ψ_2 are harmonic functions. A^I and B^I are constants to be determined. In terms of Equation 6, all the stress components can be calculated (36). The vanishing shear stresses at the plate surfaces as expressed in Equation 5 require

$$A^I = -(2\nu + CH/\tanh CH)B^I \tag{10}$$

where ν is the Poisson ratio. The constant B^I is determined from the boundary condition (4), in terms of Equations 6 and 10 as follows:

$$B^I = 2D^IF^I\sinh CH/C^3 \tag{11}$$

where

$$F^{I}(2CH) = (\sinh 2CH + 2CH)^{-1} \tag{12}$$

The constants in the symmetrical Love's strain function (6) have thus been determined. In terms of the function (6), an important normal stress of the basic symmetrical problem at an arbitrary point can be written as:

$$\bar{\sigma}^{I}_{xx} = 2D^{I}F^{I}\sinh CH\{2\nu\eta^{2}\cosh Cz + \xi^{2}[(1 - CH\coth CH)\cosh Cz + Cz\sinh Cz]\}\cos(\xi x)\cos(\eta y)/C^{2} \tag{13}$$

The above normal stress is important because it gives the stress distribution in the crack plane in the experiments described.

The similar component of the normal stress in the antisymmetrical basic problem will be described next. For the antisymmetrical basic problems, the boundary conditions are prescribed as:

$$\bar{\sigma}^{II}_{zz} = \pm D^{II}\cos\xi x\cos\eta y \quad \text{at} \quad z = \pm H \tag{14}$$

and

$$\bar{\sigma}^{II}_{zx} = \bar{\sigma}^{II}_{zy} = 0 \quad \text{at} \quad z = \pm H \tag{15}$$

The antisymmetrical Love's strain functions are chosen as follows:

$$Z^{II} = A^{II}\psi_1 + B^{II}Cz\psi_2 \tag{16}$$

where the harmonic functions ψ_1 and ψ_2 are defined respectively in Equations 7 and 8. In terms of Equation 16, the condition in Equation 15 requires

$$A^{II} = -(2\nu + CHtanhCH)B^{II} \tag{17}$$

In terms of Equations 16 and 17, the other constant is determined from the boundary condition (14) as follows:

$$B^{II} = 2D^{II}F^{II}coshCH/C^3 \tag{18}$$

where

$$F^{II}(2CH) = (sinh2CH - 2CH)^{-1} \tag{19}$$

In terms of Equations 16, 17, and 18, the antisymmetrical normal stress is written as:

$$\bar{\sigma}^{II}_{xx} = 2D^{II}F^{II}coshCH\{2\nu\eta^2 sinhCz + \xi^2[(1 - CH\ tanhCH)sinhCz + CzcoshCz]\}cos(\xi x)cos(\eta y)/C^2 \tag{20}$$

Equations 13 and 20 can be combined to form the solutions related to the experiments.

To construct the solutions of the problem, the expression for a general step function of finite length is written from the cosine Fourier transform (37) as follows:

$$[H(x-L+\varepsilon)-H(x-L-\varepsilon)]/2\varepsilon = \int_0^\infty (\pi\varepsilon\xi)^{-1}\sin\xi\varepsilon\cos[\xi(x-L)]d\xi \quad (21)$$

Equation 21 becomes $\delta(x - L)$ if ε tends to zero. In terms of Equation 21, the symmetrical boundary condition (Equation 1) can be written as integrals over the cosine functions. Using the principle of superposition, the symmetrical component of the normal stress of the problem corresponding to Equation 1 can be written from Equations 4, 13 and 21 as the limiting value for vanishing ε_1 and ε_2' of the following equation:

$$\sigma_{xx}^I = -P/\pi^2\int_0^\infty\int_0^\infty F^I\sinh CH\sin\xi\varepsilon_1/\varepsilon\xi_1 C^2$$

$$\times\{2\nu\eta^2\cosh Cz + \xi^2[(1-CH\coth CH)\cosh Cz + Cz\sinh Cz]\}$$

$$\times\{\cos(\xi x)\cos(\eta y)\sin(\eta\varepsilon_2')/\eta\varepsilon_2' + [\cos\xi(x+L)+\cos\xi(x-L)]\cos(\eta y)$$

$$\times \sin(\eta\varepsilon_2)/2\varepsilon_2\eta\}d\xi d\eta \quad (22)$$

Similarly, the antisymmetrical component of the normal stress corresponding to the boundary conditions Equation 3 is written in terms of Equations 14, 20 and 21 as the limiting value for vanishing ε_1 and ε_2' of the following equation:

$$\sigma_{xx}^{II} = -P/\pi^2 \int_o^\infty \int_o^\infty F^{II} \text{coshCHsinh}\xi\varepsilon_1 / C^2\xi\varepsilon_1$$

$$\times\{2\nu\eta\text{sinhCz} + \xi^2[(1-\text{CHtanhCH})\text{sinhCz} + \text{Czcoshz}]\}$$

$$\times\{\cos(\xi x)\cos(\eta y)\sin(\eta\varepsilon_2')/\eta\varepsilon_2'$$

$$-[\cos\xi(x+L)+\cos\xi(x-L)]\cos(\eta y)\sin(\eta\varepsilon_2)/2\varepsilon_2\eta\}d\xi d\eta \qquad (23)$$

The sum of Equations 22 and 23, i.e., $\sigma_{xx} = \sigma_{xx}^{I} + \sigma_{xx}^{II}$, give the total normal stress of the problem. If the value of x is equal to zero, the sum, σ_{xx}, gives the stress distribution on the crack plane in the experiments. Along the lower edge of the crack plane, the normal stress is obtained by integrating Equations 22 and 23 at z = -H and x = 0 as follows:

$$\sigma_{xx}(0,y,-H) = -PQ + (1-2\nu)PN/2\pi + P/\pi^2 \int_o^\infty \int_o^\infty [\eta\varepsilon_2 + \text{sinn}\eta\varepsilon_2]F^{I}$$

$$+ (\eta\varepsilon_2 - \text{sinn}\eta\varepsilon_2)F^{II}](\xi^2 + \nu\eta^2)(C^2\eta^2\varepsilon_2)^{-1} 2\text{CHcos}\eta y\cos\xi L d\eta d\xi \qquad (24)$$

where

$$N = \{(y+\varepsilon_2)[L^2+(y+\varepsilon_2)^2]^{-1} - (y-\varepsilon_2)[L^2+(y-\varepsilon_2)^2]^{-1}\}/2\varepsilon_2 \qquad (25)$$

The symmetrical component of the normal stress along the upper and lower edges of the crack plane is obtained from Equation 22 through integrations at z = $\pm$ H and x = 0 as follows:

$$\sigma^{I}_{xx}(0,y,H) = -P\delta(x)\delta(y)/2 - PQ - (1-2\nu)P(y^{-2}-N)/4\pi$$

$$+ P/\pi^2\int_0^\infty\int_0^\infty MCH[1 - (1 - \nu)\eta^2/C^2]d\xi d\eta \qquad (26)$$

where

$$M = 2(1+\sin(\eta\epsilon_2)\cos(\xi L)/\eta\epsilon_2)F^{I}\cos\eta y \qquad (27)$$

Inside the plate where $z < H$, the symmetrical component is written also from Equation 22 at $x = 0$ as:

$$\sigma^{I}_{xx}(0,y,z) = -P/2\pi^2\int_0^\infty\int_0^\infty MsinhCH\{coshCH[1 - (1 - 2\nu)\eta^2/C^2]$$

$$+ \xi^2(CzsinhCz - CHcoshCz/tanhCH)/C^2\}d\xi d\eta \qquad (28)$$

To obtain the numerical values of the crack plane normal stresses, the transformations $\xi = U\sin\theta/2H$ and $\eta = U\cos\theta/2H$ are introduced into Equations 24, 26, and 28. After the transformations, the double infinite integrals reduce to a single infinite integration over U from 0 to ∞ and a finite integration over θ from 0 to $\pi/2$. Furthermore, all space variables are normalized by 2H, and the stresses can be written as the product of a dimensional quantity $P/(2H)^2$ and a nondimensional function. The nondimensional functions are calculated by the techniques similar to those used in (35), using an IBM 360/65 computer. The values of the total tensile stress in Equation 24 along the lower and upper edges of the crack plane are

calculated and normalized by the maximum tensile stress $\sigma_o = \sigma_{xx}(0,0,-H)$ in the lower plate surface at the center of the support. The results are expressed in terms of the non-dimensional parameters involved in Fig. 4a. The symmetrical component of the stress is symmetrically distributed with respect to the midplane of the plate, and its values are calculated for $z/2H = 0.5$ from Equation 26 and for $z/2H = 0$ and 0.25 from Equation 28. The calculated values are then integrated over the thickness using Simpson's rule to obtain the in-plate stretching force per linear length of the crack. The stretching force is finally divided by the plate thickness, 2H, to obtain the averaged in-plane stretching stress.

For the other experimental arrangement, the axisymmetrical stress field produced by an indenter in a plate supported by a ring foundation can be obtained from the results in (35). The loads produced by the indenter and the ring support are respectively considered as a concentrated load P and a circular line load. The boundary conditions can be written in cylindrical coordinates (r,ϕ,z) as the sum of the following two parts (35):

$$\text{Sym:} \quad \sigma_{zz}^{I} = -P[\delta(r) + \delta(\rho-r)]/4\pi r, \quad z = \pm H \tag{29}$$

$$\text{Antisym:} \quad \sigma_{zz}^{II} = \mp P[\delta(r) - \delta(\rho-r)]/4\pi r, \quad z = \pm H \tag{30}$$

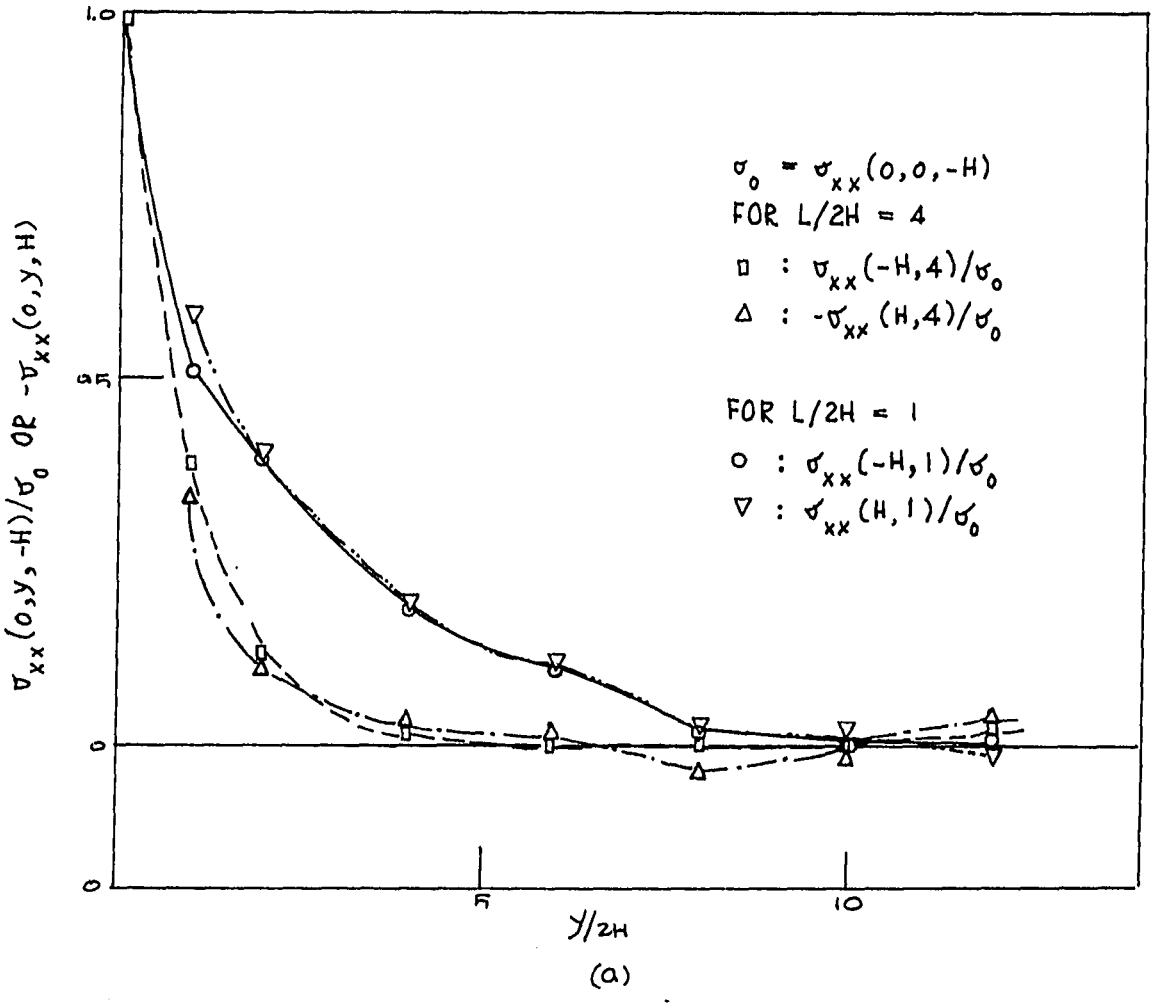

(a)

Fig. 4a. Total stress in the surface of the specimen supported by the knife-edged foundation

where ρ is the radius of the ring support. The total circumferential component of the stress at the lower plate surface $z = -H$ can be written from Equation 33 of (35) in terms of the zeroth order Hankel transform of Equations 29 and 30, as follows:

$$\sigma_{\phi\phi} = -[2\nu\delta(\rho-r)+(1-2\nu)H(r-\rho)/r]P/2\pi r + \bar{S} \tag{31}$$

where

$$\bar{S} = P/4\pi \int_0^\infty G\{[1+J_o(S\rho)]F^I + [1-J_o(S\rho)]F^{II}\}2HS^2dS \tag{32}$$

and

$$G = (1-\nu)J_2(Sr) + (1+\nu)J_o(Sr) \tag{33}$$

The argument of both F^I and F^{II} is 2Hs. J_o and J_2 are, respectively, the zeroth and the second order Bessel functions. The symmetrical stress component $\sigma^I_{\phi\phi}$ is obtained from Equation 26 of (38) if $\bar{p}$ in that equation is replaced by the negative value of the zeroth order Hankel transform of Equation 29 as follows:

$$\bar{\sigma}^I_{zz} = -P[1 + J_o(S\rho)]/4\pi \tag{34}$$

In the plate surface, the stress is obtained as follows:

$$\sigma^I_{\phi\phi}(r,H) = P\{2\nu[\delta(r)+\delta(\rho-r)]+(1-2\nu)[H(r)+H(r-\rho)]/r\}/4\pi r + \int_0^\infty GF^I\,\bar{\sigma}^I_{zz}\,2HS^2dS \tag{35}$$

Using the transformation S = U/2H and normalizing all the space variables by 2H, $\sigma_{\phi\phi}$ in Equation 31 and $\sigma^{I}_{\phi\phi}$ inside the plate and on the surface in Equation 35 can all three be written as the product of $P/(2H)^2$ and a nondimensional function, as in the case of the knife-edged support. $\sigma_{\phi\phi}$ has a behavior similar to σ_{xx}. $\sigma^{I}_{\phi\phi}$ at various depths is calculated and averaged to obtain the average in-plane stretching stress $\bar{\sigma}_{\phi\phi}$ which is similar to $\bar{\sigma}_{xx}$. The values of $\bar{\sigma}_{\phi\phi}$ normalized by $\sigma_o = \sigma_{\phi\phi}(0,-H)$ are also expressed together with $\bar{\sigma}_{xx}$ Fig. 4a-4b.

C. Results

The oscilloscope traces for measuring the flexure crack speeds of glass plates were photographed and shown in Fig. 2a-2d. By measuring the trace length which gives the time interval required to break the silver lines from one to another, the crack speeds were obtained by dividing the distance between silver lines by the corresponding trace length. The curves of crack speeds vs. distance measured from the point of loading were obtained and plotted in Fig. 5, in the averaged sense between two consecutive silver lines. The curves of normalized total surface stress and normalized in-plane averaged stretching stress vs. distance measured from the point of loading were also obtained and plotted in Fig. 4a and Fig. 4b respectively.

The crack speeds varied from 36 m/sec to 476 m/sec, which were small compared to the limiting crack speed of 1500 m/sec

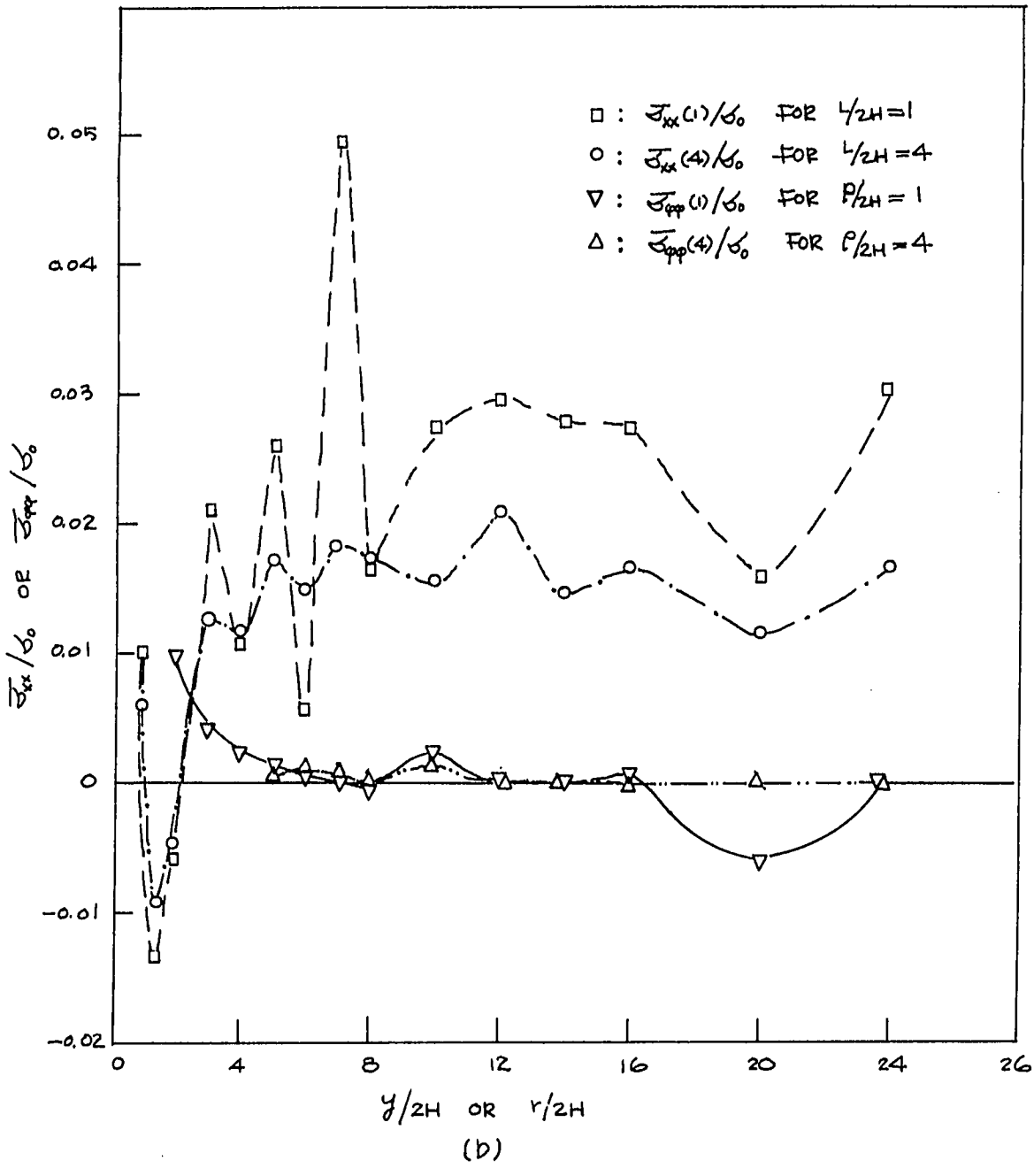

(b)

Fig. 4b. In-plane average stretching stress

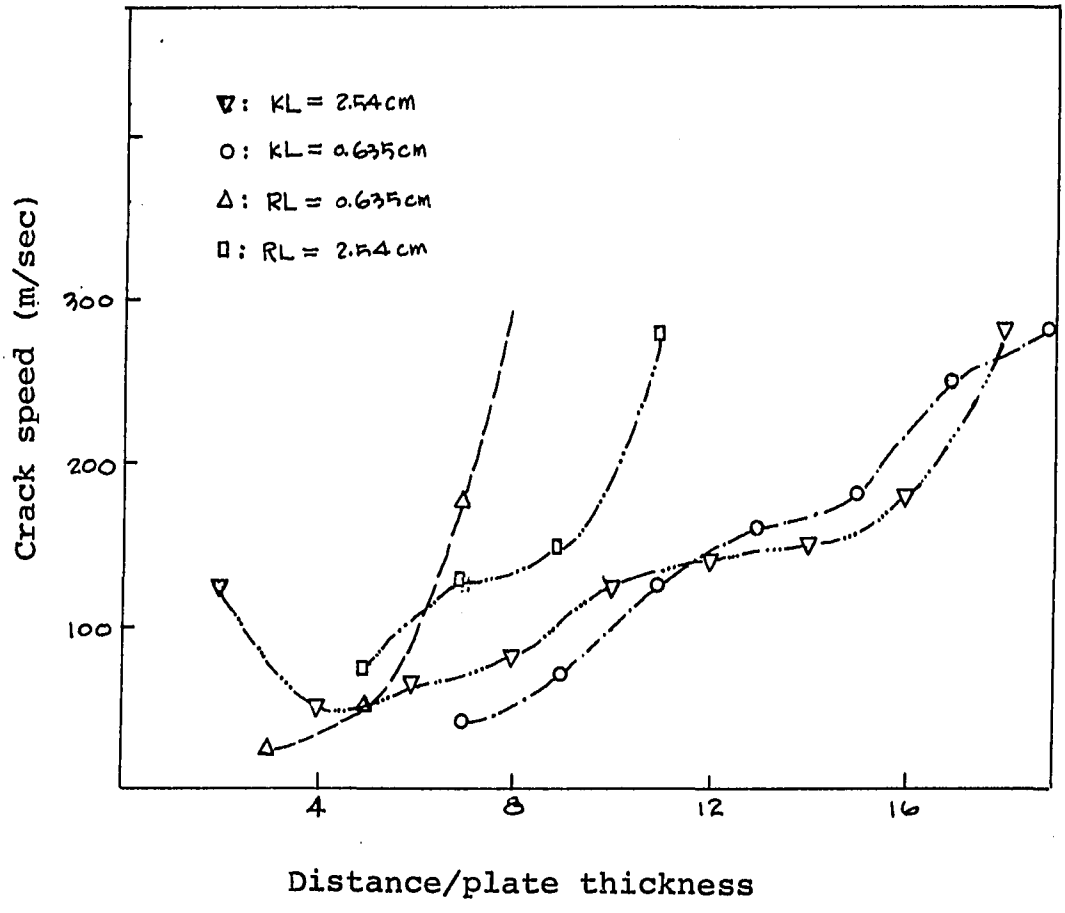

Fig. 5. Flexure crack speed measured experimentally at various distance from the loading point

(1). It was observed experimentally for the knife-edged supports that the fracture picked up speed very quickly in the initial stage, and then slowed down a certain amount and finally accelerated again until the specimen was completely ruptured. The photograph in Fig. 2a shows the deceleration and acceleration of the fracture produced for the knife-edged support of the 2.54 cm span. The other photographs show the final stage of acceleration. Nearby the knife-edged support of the 0.635 cm span, the crack speed was observed to be so slow that no settings of the oscilloscope could be selected to measure the complete variation of the speeds over the distance covered by the grid. Therefore, the grid was placed a distance away from the support where the speeds were more comparable in magnitude and became measurable as shown in Fig. 2b. The slowdown of the crack speed nearby the support was shown in Fig. 2b to be a result of the condition that the crack was running in a compressive in-plane stress zone. The zone of the compressive in-plane stress does not occur nearby the ring support of 0.635 cm radius. Therefore, the crack speeds were measured as shown in Fig. 2a for the distance closer to the support than to the 0.635 cm knife-edged support.

The fracture for the knife-edged supports used was observed to be running linearly in the direction of the scratch which is along the centerline of the specimen. Due to the axisymmetrical nature of the pre-fracture stress distribution

in the specimens on the ring supports, the fracture was observed as cross-shaped running in two mutually perpendicular directions, one being in the direction of the scratch introduced. The specimens on the ring foundations appear to have been further weakened by the double fracture so that the crack speeds measured were higher than those for the knife-edged supports of comparable span as shown in Fig. 5. Furthermore, the cross-shaped fracture had a significant effect on the crack speeds for the 0.635 cm ring support that the crack ran at an extremely high rate toward the final stage of rupture as shown in Fig. 2d. This is consistent with the fact that the crack speed in glass plates increases at a high rate to a limiting value as observed previously (1, 2).

The values of $\bar{\sigma}_{xx}$ are very small compared to the maximum tensile stress σ_o and are expressed in terms of the nondimensional parameters in Fig. 4b. The magnitudes of the total tensile and compressive surface stress can be seen in Fig. 4a to be decreasing very rapidly with increasing distance from the center of the support. Their magnitudes eventually become comparable to the small values of the averaged stretching stresses at distances far away from the loading point. Furthermore, the averaged stretching stress is compressive in the range where y/2H is about equal to 1.2 to 1.4. It appears that the maximum tensile stress at the center of the support in the lower plate surface is the governing factor for the initiation

of the flexure fracture as was observed previously (35). Once the flexure has started, it quickly becomes a through-the-thickness crack running in the total crack plane stress field, which is positive on one surface and negative on the other surface. Furthermore, one of the total surface stresses for 2L = 2.54 cm remains tensile and of relatively high value (Fig. 4a) in the range where the crack speed was measured to be decreasing (Fig. 4a). Therefore, the total stress does not seem to correlate to the slowdown of the cracks observed experimentally. It is the averaged stretching stress $\bar{\sigma}_{xx}$ which is compressive near the knife-edged support (Fig. 4b). In the neighborhood of the 2.54 cm knife-edged support, the crack speed was measured to be decreasing (Fig. 5). For y/2H larger than 6 in Fig. 4b, $\bar{\sigma}_{xx}$ for 2L = 0.635 cm is larger than that for 2L = 2.54 cm. In this range the crack speed for 2L = 0.635 cm was measured to be increasing faster than that for 2L = 2.54 cm. In general, the stretching stress $\bar{\sigma}_{xx}$ is small, so that the crack acceleration is also small and becomes measurable as in Figs. 2 and 5. The values of $\bar{\sigma}_{\phi\phi}$ normalized by σ_o are also expressed together with $\bar{\sigma}_{xx}$ in Fig. 4b and do not show any compressive zone close to the ring supports. Therefore, the crack speeds for the support of 0.635 cm radius were measurable close to the support as shown in Fig. 5. For the knife-edged support of 0.635 cm span, the crack speeds were slowed down significantly in the compressive zone nearby the

support so that the crack speed could not be measured close to the support as explained before. This again confirms the existence of the compressive in-plane stress nearby the support and its slowdown effects on the crack speed.

IV. PROPAGATION AND SURFACE ENERGY OF FLEXURE CRACK IN POLYMETHYLMETHACRYLATE PLATES

The propagation of a flexure crack produced in PMMA plate by a transverse static loading is investigated. The crack speed of the flexure crack was measured experimentally.

The surface energy of PMMA plate due to quasi-static and impact loadings is investigated. For the case of a quasi-static loading, the curve of loading vs. deflection was measured experimentally and so was the crack length. For the case of an impact loading, the curve of acceleration vs. duration time was traced experimentally and the crack length was also measured.

A. Crack Propagation

The experimental set-up, procedure and measurement of crack speed were the same as those of glass plates except the glass plates were replaced by the PMMA plates.

1. Measurement of crack speed

Observations were made on flexure cracks running along the center line of PMMA plates which rested on the top of a ring or double knife-edged foundation and experiments were carried out to measure the crack speeds in PMMA plates.

The set up of experiment was similar to that for glass plates and shown in Fig. 1a, b and the electrical circuitry

used was shown in Fig. 1c. A steel ball of 1 $\frac{3}{4}$" diameter was fixed to an adapter (see Fig. 1a) which in turn screwed into the top plate of the hydraulic press. All specimens are 1/8" x 3" x 7". Three different ring foundations (1/4", 1/2" and 1" diameter) and three different double knife-edged foundations (1/4" x 1/4", 1/4" x 1/2" and 1/4" x 1") (Fig. 1a, b) were used. A system of electrical circuitry was required for the test. D.C. source was a six volt Eveready D.C. battery. A Tektronix type 502A dual beam oscilloscope with Tektronix C-12 camera was also used. All external cables were shielded and grounded.

All the specimens were cut from the same ® Plexiglass plate without scratch. The dimensions of the PMMA plates are 17.78 x 7.62 x 0.3175 cm for all the specimens. Acetone was used to clean the surface of the PMMA plate before depositing the silver film. Scratches were introduced in the specimens as was done for the glass specimens. In front of the scratch, 10 silver lines (2" long, 1/4" wide, 600 Å thick) of 6.35 mm (center to center) apart were deposited by using a vacuum evaporator. The lines were perpendicular to the direction of the scratch which is the expected direction of fracture. At each end of the silver film grid the electrical terminal was fixed with 5 minute epoxy. Eleven shielded electrical wires were plugged into a control box (as Fig. 1c) and connected to the electrical terminals. Furthermore, an electrical wire was used to feed

the signal output from the control box into the oscilloscope. During the experiment, the procedure was just the same as that of glass case except that the glass plate was replaced by PMMA plate.

2. Results

The oscilloscope traces for measuring the flexure crack speeds of PMMA plates were photographed and shown in Figs. 6a-6d. The method of calculating the averaged crack speed is the same as that in glass plates. The curves of crack speeds of PMMA plates vs. distance measured from the point of loading were obtained and plotted in Fig. 7.

The crack speeds varied from 1.3 m/sec to 13 m/sec and were small compared to the crack speeds of the previous glass specimens, which ranged from 36 m/sec to 476 m/sec. Since the in-plane stretching stress in the PMMA specimen was small, the crack speeds measured were also small compared to the limiting crack speed of 670 m/sec (39) as was the case for the glass specimens. The surface energy of PMMA is known to be about 1000 times as high as that of glass. This high value of the surface energy would cause a relatively large resistance to the propagation of a crack in PMMA. As a result, it can be seen in Fig. 7 that the crack speeds in the PMMA plates increased slowly in the initial stages, and then oscillated at low frequencies until the specimens were completely fractured.

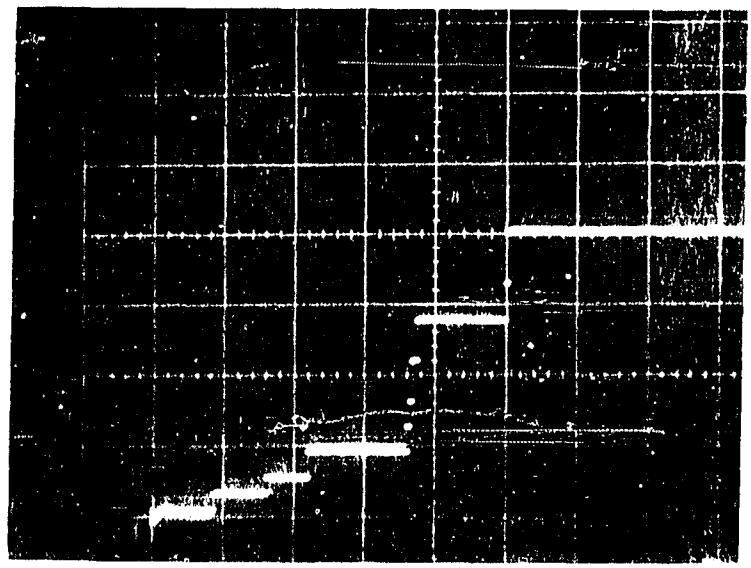

(a) 5 msec

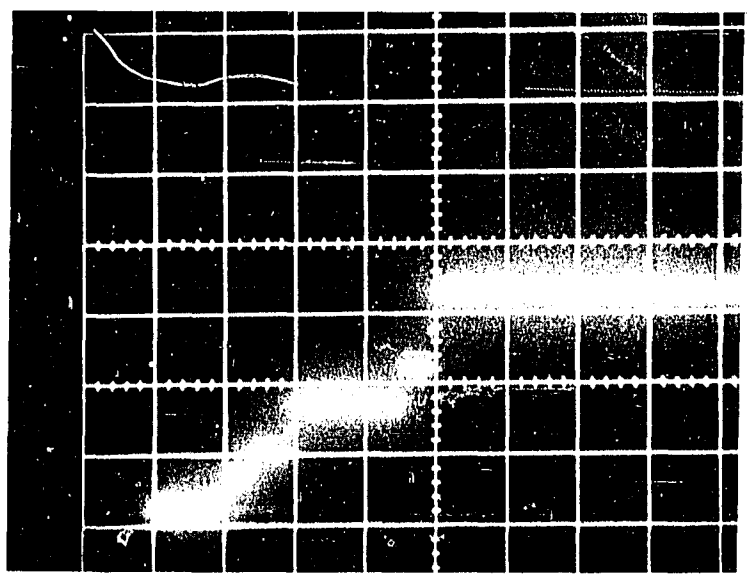

(b)

Fig. 6 Oscilloscope trace measuring the flexure crack speed

(a) 2L = 2.54 cm
(b) 2L = 0.635 cm

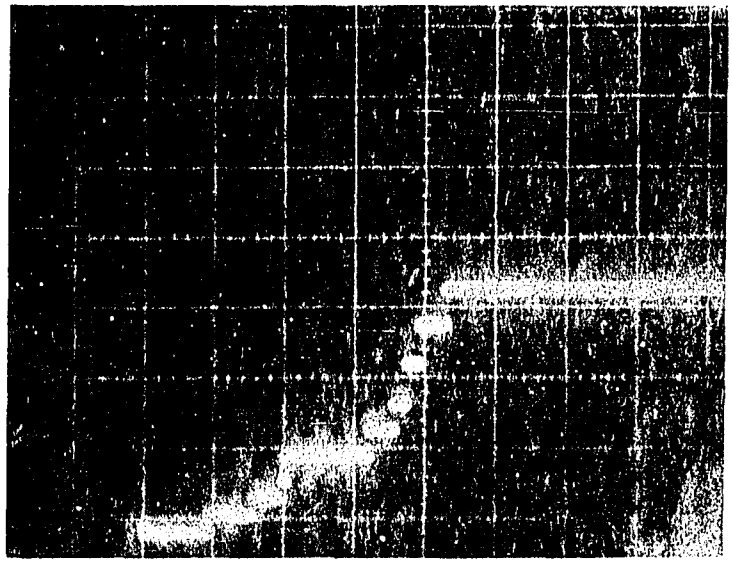

(c) 5 msec

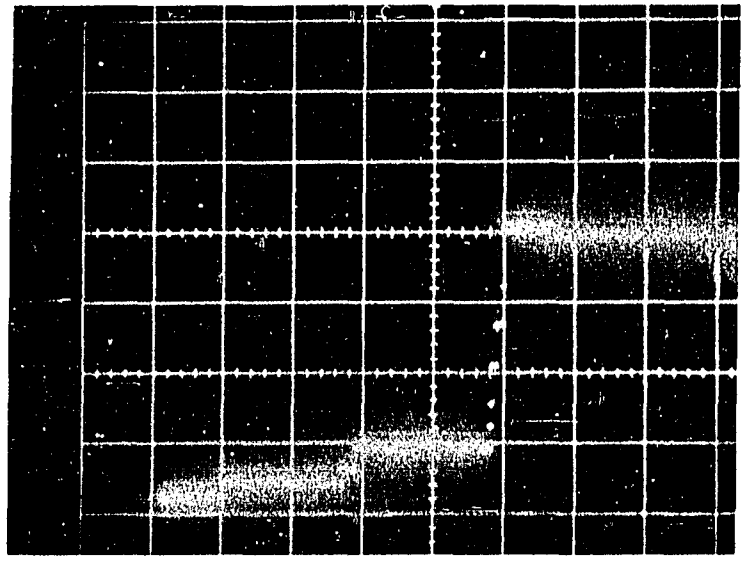

(d)

Fig. 6 (Continued)

(c) $2\rho = 2.54$ cm
(d) $2\rho = 0.635$ cm

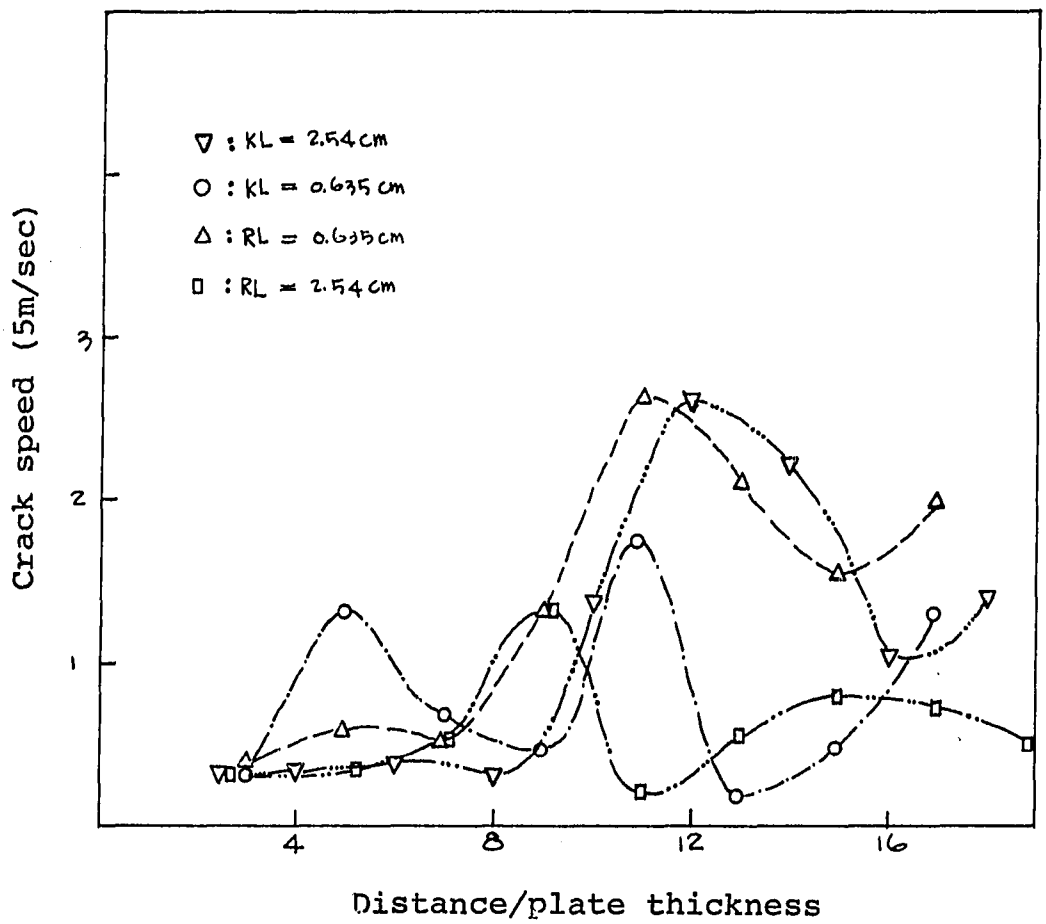

Fig. 7. Flexure crack speed measured experimentally at various distances from the loading point

B. Surface Energy

As determined for two-dimensional states of stress under static loading, the surface energy for a PMMA plate has values ranging from 1.2×10^5 to 6.5×10^5 erg/cm^2 (40). However, the behavior of a material under static loading is generally different from that under dynamic loading, and the value of the surface energy under dynamic loading is not known. In the present work, experiments are described to determine the surface energy in a PMMA plate under quasi-static and dynamic loading.

1. Quasi-static surface energy

Surface energy of PMMA plates subjected to slow transverse loads were measured using an experimental set-up similar to that used for the previous crack-speed measurements.

a. Experimental set-up and procedure The experimental set-up was shown in Fig. 8. A MTS machine (series 810) was used for this test. Clean and polished circular PMMA plates (4" diameter, 1/16" thick) were used as specimens. A system as shown in Fig. 8 was designed to adapt a steel ball of $1\frac{3}{4}$" diameter to the MTS machine for loading the specimens. The ring foundation with diameter 1" was employed to support the lower surface of a specimen. The steel ball of diameter $1\frac{3}{4}$" was held by the system of the adapter which was connected to the cross-head of the MTS machine. The ring

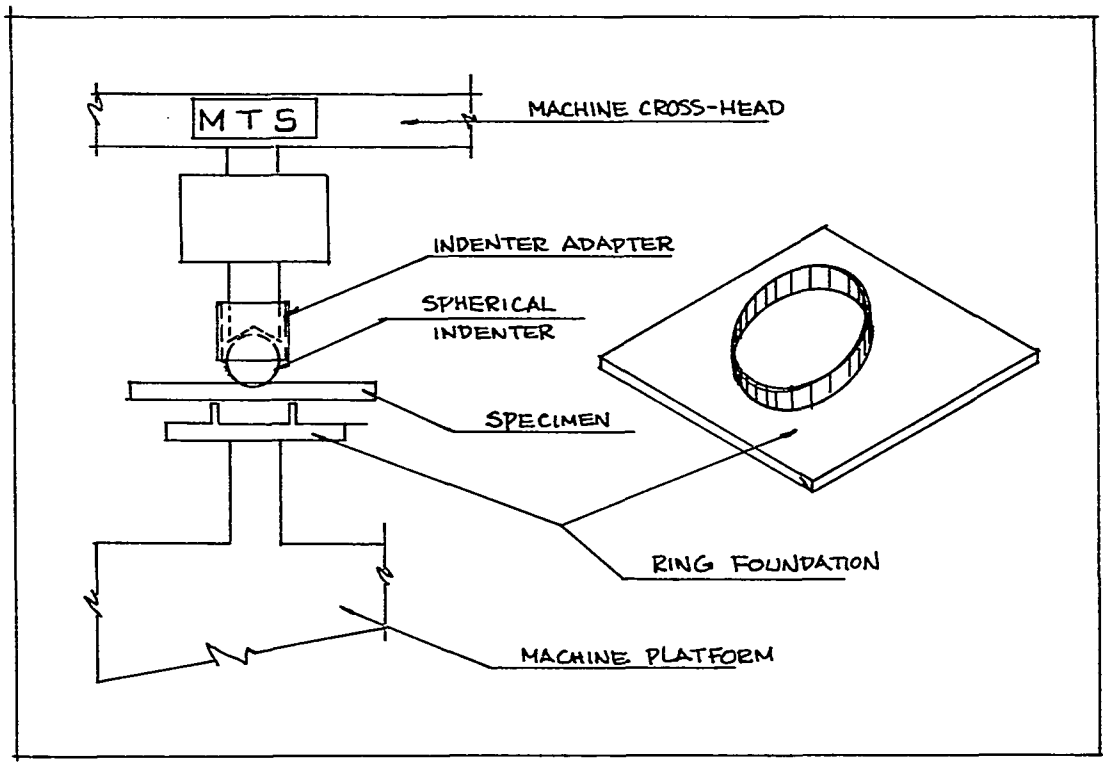

Fig. 8. Experimental set-up for measuring surface energy of PMMA plate

foundation was placed on the platform of the MTS machine. The out-put of the machine was recorded on properly scaled graph papers. The center of the PMMA plate was aligned with the center of the ring foundation and the center of the steel ball. A space of about one inch was left between the lowest point of the steel ball and the upper surface of the specimen before load was applied. The stroke control was properly chosen. The machine was operated to press the steel ball onto the upper surface of PMMA plate and the MTS machine automatically plotted the curve of loading vs. deflection. Once fracture occurred, the machine was unloaded immediately. From the fractured specimen, crack surfaces were measured.

b. Results The load-deflection curve obtained from the MTS machine is shown in Fig. 9. From the curve, the load P required to fracture the specimen was determined to be 42.5 lb. The corresponding deflection δ was determined as 0.0197". At the instant just before the fracture occurred, the work done on the specimen is equal to $P\delta/2$. This work was stored as strain energy in the specimen. When the fracture occurred, new material surface was created and strain energy was released and converted into the surface energy of the newly created material surface. From the balance of energy, an equation for determining the surface energy is established as follows:

$$P\delta/2 = 2\gamma hC \tag{36}$$

where γ is the surface energy, h the plate thickness, and C the total crack length. From the fractured specimen of 1/16"

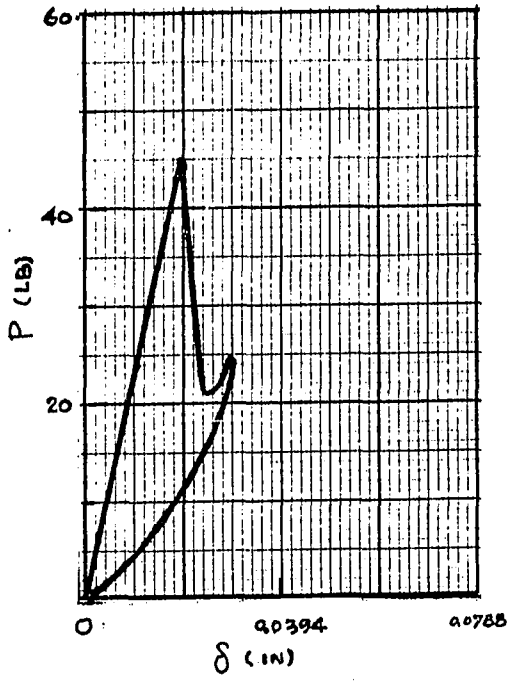

Fig. 9. Load-deflection curve

thickness, the total crack length was measured as 1.25". The shape of the crack can be drawn as shown in Fig. 10. From Equation 36 with the values measured above, the static surface energy is determined to be 4.62×10^5 erg/cm^2. This value is very comparable to that mentioned above (39).

2. Dynamic surface energy

Study of the dynamic behavior of a material is in general more complicated than for a static loading. A new experimental system was designed and used to determine the surface energy of a PMMA plate under an impact loading.

a. Experimental set-up and procedure The experimental set up is shown in Fig. 11. The basic equipment used in this test consisted of an impact system, a power supply, a Tektronik oscilloscope with camera, an accelerometer mounted on a partially cut steel ball, a photo-cell system and a magnetic system. The impact system was designed and fabricated from a steel cubical block 9" x 9" x 7". It was placed on a 3' high support for stability. A 2" diameter by 2" deep hole was machined in the central part of one face of the steel block for adapting a foundation. A ring foundation of 1" diameter was built and heat treated for using in the impact test. Also, a steel frame (Fig. 11) was built so that the steel ball could be suspended from a fine nylon wire at various heights. The steel ball and fine nylon wire behaved like a pendulum. A two-legged pendulum system was used to prevent sidesway of the

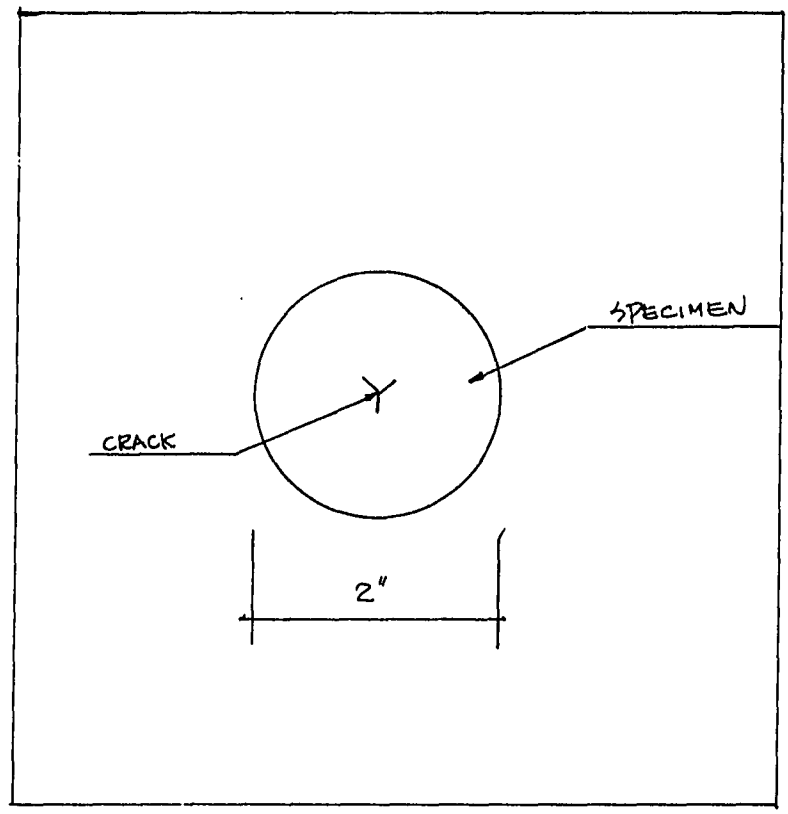

Fig. 10. The shape of crack

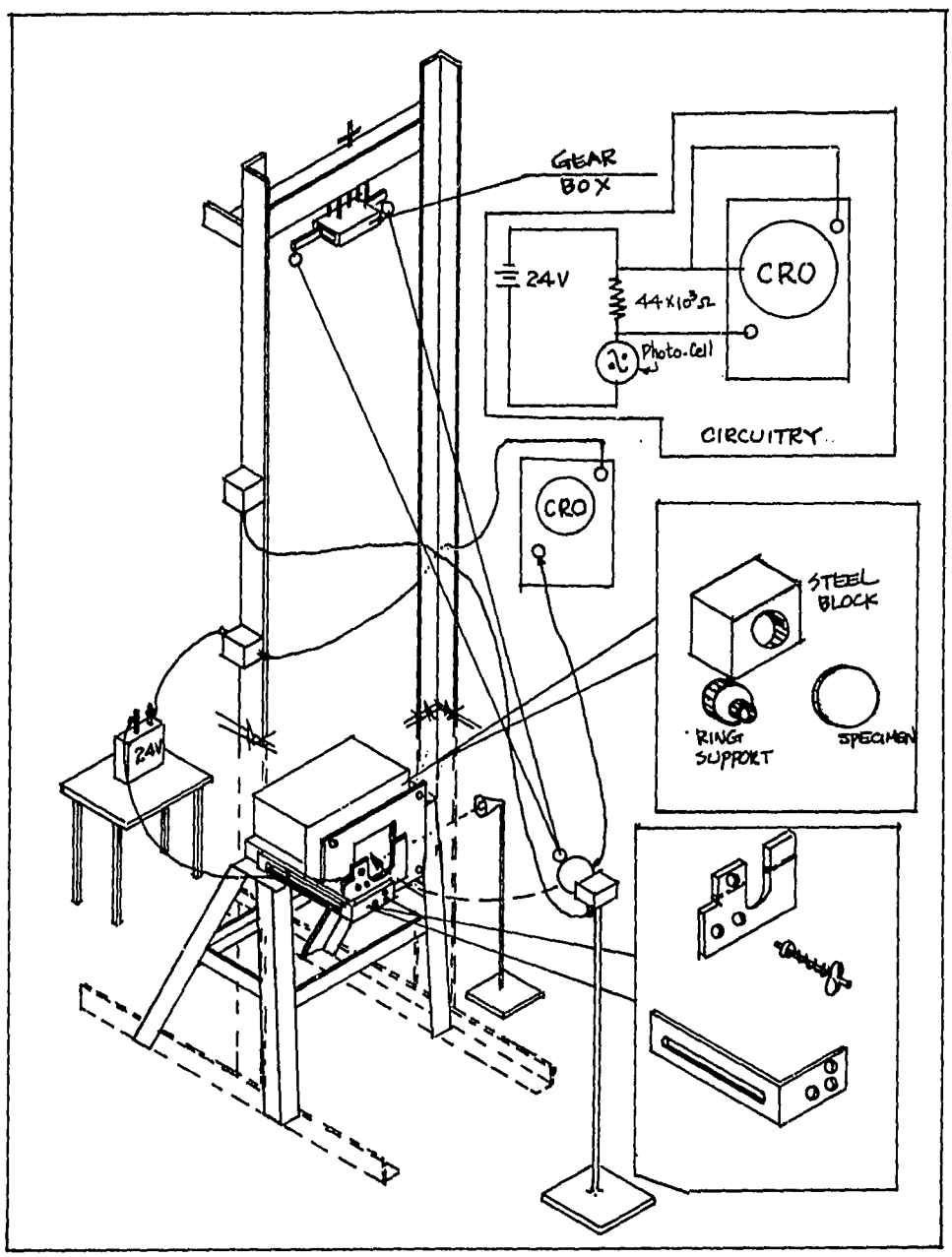

Fig. 11. Experimental set-up for impact loading

ball before impact. A gear-box (Fig. 11) apparatus was used make both vertical and horizontal alignments. A portion of the steel ball which had the weight equal to that of the accelerometer was cut off and the accellerometer was screwed onto the flat cut-off side of the steel ball. At the free end of the accelerometer, a thin steel plate (Fig. 11) was glued to prevent the disturbance of the accelerometer from the magnetic action between the accelerometer and the magnetic system. An electromagnet was custom-made from a Guardian Series 200-relay coil assembly, 6V D.C., No. 200-6D. A steel ball (1/2" diameter) was placed in contact with the magnet and the entire assembly (Fig. 11) was contained in an aluminum box which was free to move along a vertical steel bar which in turn was screwed down into the steel plate for support (Fig. 11). In front of the steel cubical block, a photo-cell system was built to trigger the oscilloscope (as Fig. 11). As shown in Fig. 11, one end of a steel plate was connected to a U-shaped aluminum plate. Two tiny holes (Fig. 11) were drawn through the upper part of both legs of the U-shaped aluminum source plate. The light source was a high intensity lamp (Fig. 11) and the photo-cell was CRL IN 2175. The holes faced each other in the U-shaped aluminum plate whose position could be adjusted horizontally by using three sets of springs, threads and wing nuts. The photocell was connected to a box system (as Fig. 11) with two outlets, one to a D.C. (24 volts) supply, the other to D.C. level of the oscilloscope. In the back face of the

impacting steel ball, the output of the accelerometer was fed with a cable (Fig. 11) to A.C. level of the oscilloscope. The magnetic system was connected to the power supply for controlling the release of the steel ball. At the four corner of the steel block, four rods with spring and nut were fixed for holding the plate (Fig. 11) which kept the specimen in position. The entire system was properly grounded. A 4" diameter, 1/16" thick PMMA plate was cut from commercial plexiglas and cleaned with Acetone. The specimen was then set on the back of the aluminum plate (Fig. 11) which rested vertically in front of the steel ball so that the specimen was in contact with the ring foundation (Fig. 11). The steel ball was placed at a specified distance from the front face of the specimen. As soon as the current in the electromagnet was switched off, the steel ball started to travel down and cut the light beam, and finally hit the specimen. The disturbance of the light intensity on the photocell generated an electrical signal which was used to trigger the oscilloscope. The impact of the steel ball on the specimen excited the accelerometer which also generated an electrical signal. The signal was fed to the oscilloscope and displayed on its screen. The signals on the screen were then recorded with the camera mounted on the oscilloscope.

b. Results The outputs of the accelerometer were photographed from the screen of the oscilloscope and are shown in Fig. 12a, b for the same impact velocity of 43.39 in/sec.

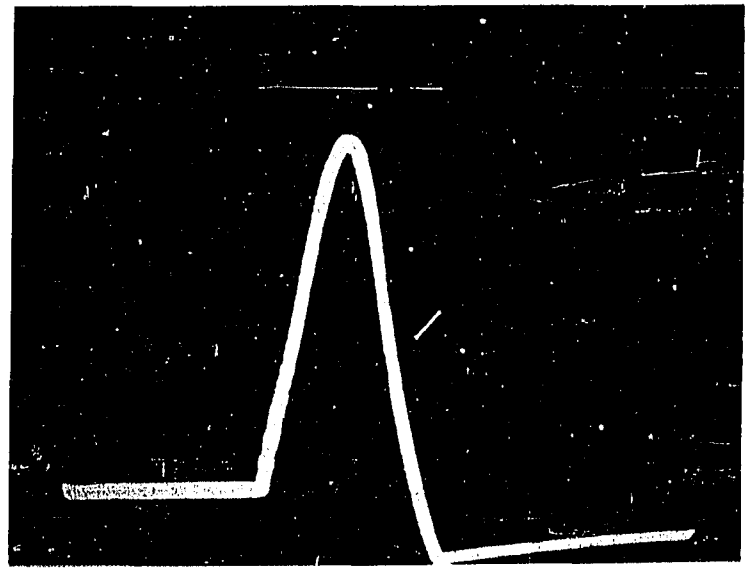

(a) 2msec

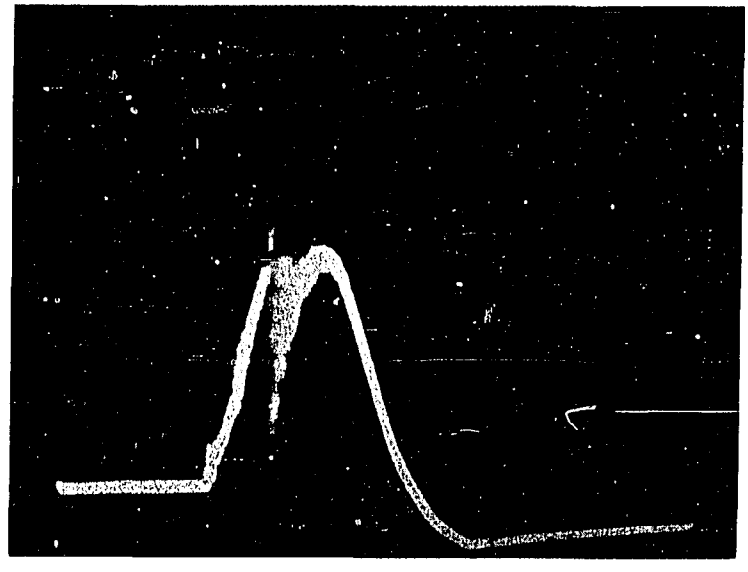

(b)

Fig. 12. Output of accelerometer

The impact velocity was purposely chosen to be at a value where the probability of occurrence of fracture is about 50 percent. The curve in Fig. 12a corresponds to the case where fracture did not occur. It can be seen that the curve is smooth and has a higher peak value than that in Fig. 12b. The occurrence of fracture clearly resulted in a sudden drop of the amplitude of the accelerometer output as shown in Fig. 12b.

After proper conversions, the curves in Fig. 13a, b are obtained from Fig. 12a, b respectively and give the acceleration of the steel ball during the impacts. If the values of the acceleration are multiplied by the mass of the steel ball, the impact forces exerted by the steel ball on the plate specimen can be obtained. The velocity of the steel ball can also be obtained from the acceleration curve if the acceleration is integrated over the time with incorporation of the initial impact velocity. The velocity curve can further be integrated to give the deflection of the plate specimen. Detailed conversions and integrations are given in Appendix A.

The maximum load for the curve in Fig. 13a was calculated as P_1 = 55 lb. At this instant, the deflection of the plate specimen was obtained as δ_1 = 0.0621 in. as shown in Fig. 14a. Thus, the strain energy stored in the specimen is $P_1\delta_1/2$, as was explained in the static case. Furthermore, this maximum load of 55 lb is considered as the averaged dynamic fracture load of the specimen, which is higher than the corresponding

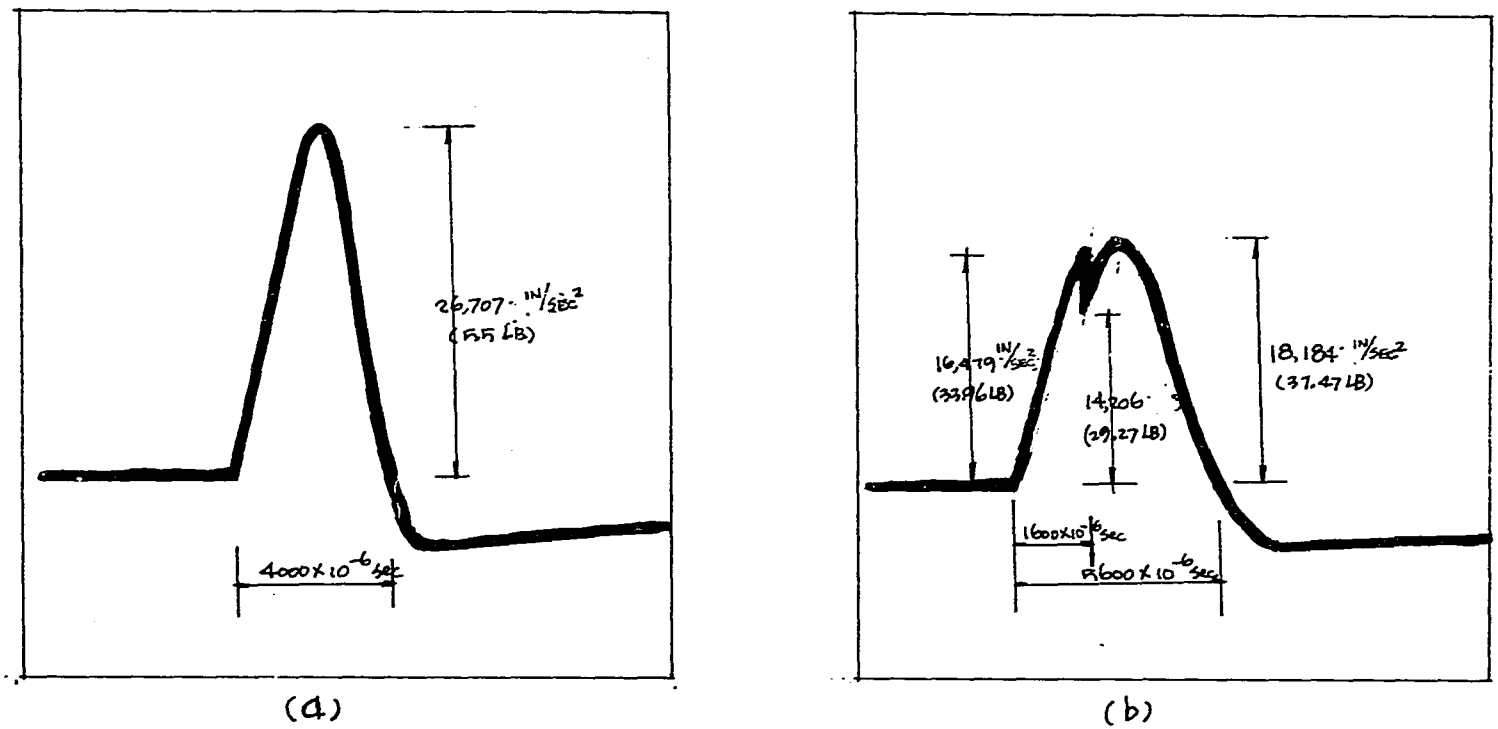

Fig. 13. Curves after conversion

static fracture load of 42.5 lb.

Because of the occurrence of fracture for the curve in Fig. 12b, the strain energy stored in the specimen was released and converted to the surface energy of the newly created fracture surface. Therefore, at the instant when the above maximum load P_1 and deflection δ_1 were determined, the impact load P_2 and the deflection δ_2 for the fracture curve shown in Fig. 14b were determined to have lower values of 33.76 lb and 0.0684 in respectively. The difference between the stored strain energies of the above two cases were converted into the energy required for forming the new fracture surface. Therefore, the balance of energy can be written as

$$\frac{1}{2} P_1\delta_1 - \frac{1}{2} P_2\delta_2 = 2\gamma_D h C_D \tag{37}$$

where C_D is the total crack length, h the plate thickness and γ_D the dynamic surface energy. The total crack length in the fractured PMMA plate specimen of 1/16" thickness was measured as 1.375". From Equation 37, the dynamic surface energy γ_D was determined as 5.55×10^5 erg/cm^2, which is higher than the corresponding static value of 4.62×10^5 erg/cm^2.

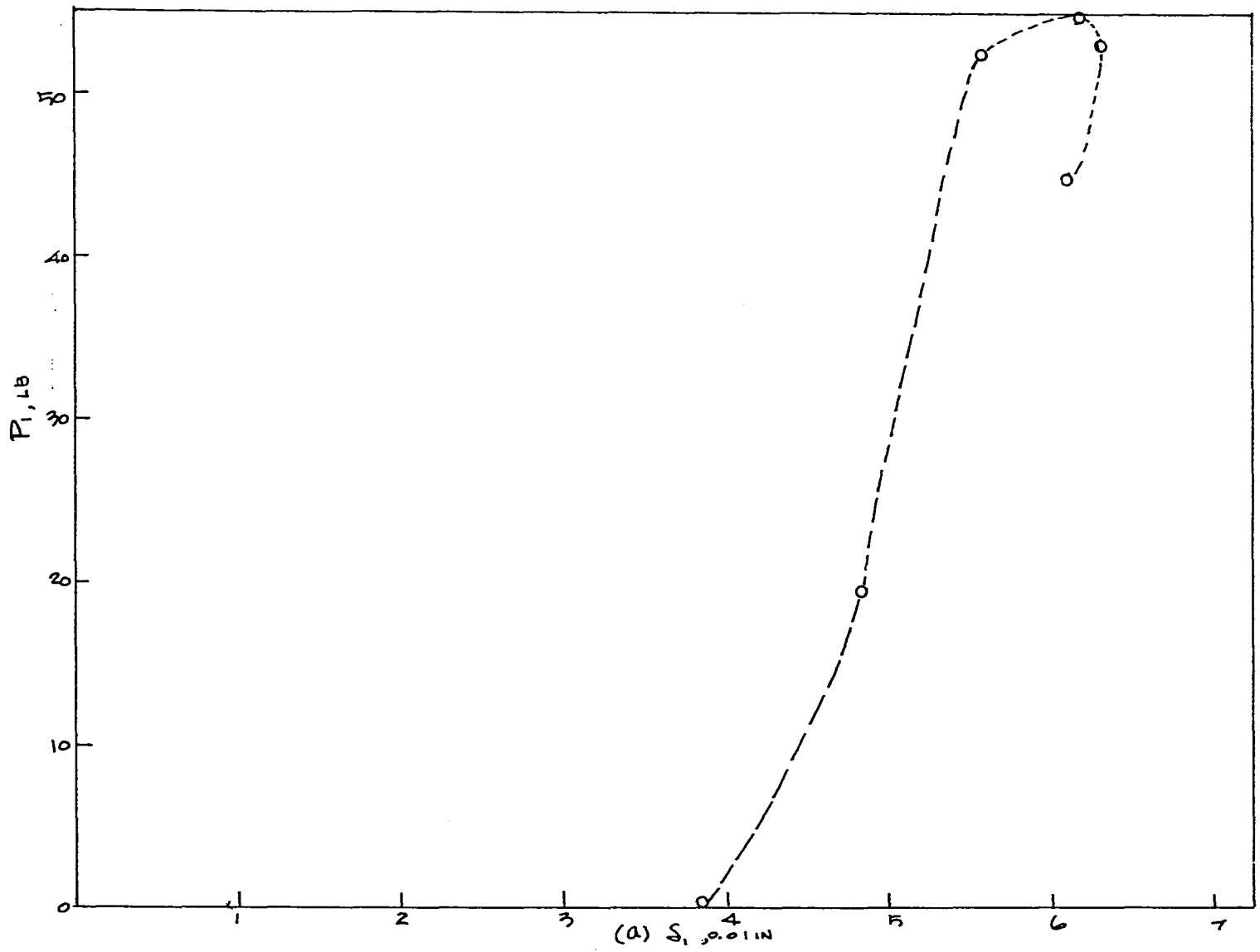

Fig. 14a. Load-deflection curve

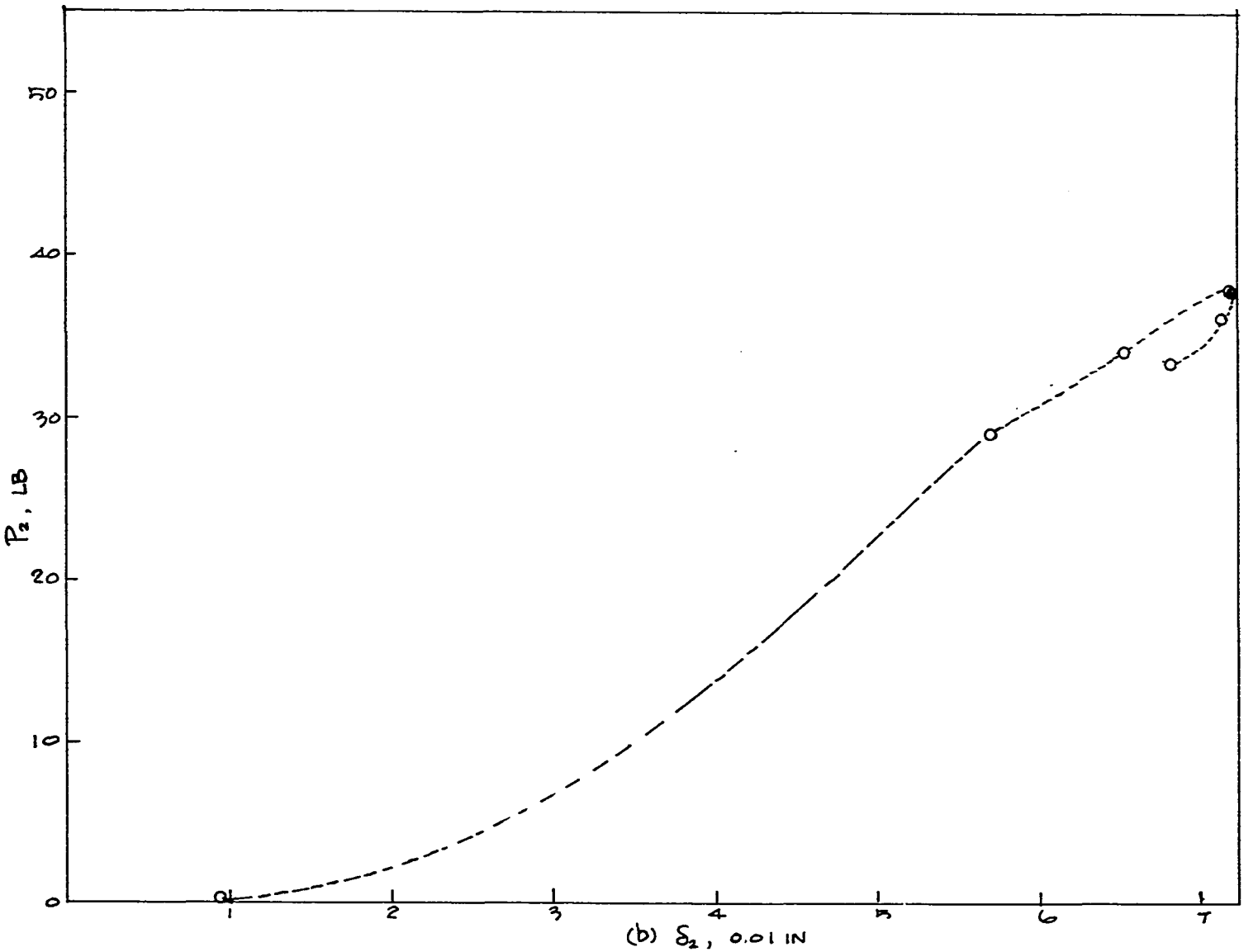

Fig. 14b. Load-deflection curve

V. HERTZIAN FRACTURE AND FLEXURE FRACTURE PRODUCED BY IMPACT IN GLASS PLATES

The stress components in a plate under the action of a transverse load can generally be split into two parts, bending and stretching. The bending part is predominating when the support span is large compared to the plate thickness. This type of problem has been investigated extensively in the literature. If the support span is reduced and becomes comparable to the plate thickness, the stretching part also becomes important in addition to the bending effects. It was in this range of the ratio between plate thickness and support span that a contact problem for static loading was investigated both theoretically and experimentally (35). Both Hertzian fracture and flexure fractures were observed for 1/8" thick glass plates (35). The above static problem is to be extended to dynamic loadings. Emphases are placed on the range where the transition from Hertzian fracture to flexure fracture occurs.

A. Experimental Set-Up and Procedure

A steel ball of $1\frac{3}{4}$" diameter was allowed to fall freely onto the upper surface of a glass plate specimen which was laid horizontally on the top of ring foundations of various diameters (Fig. 15). The ring foundations were mounted on the different faces of a steel block 6" x 7" x 6" with 5 minute

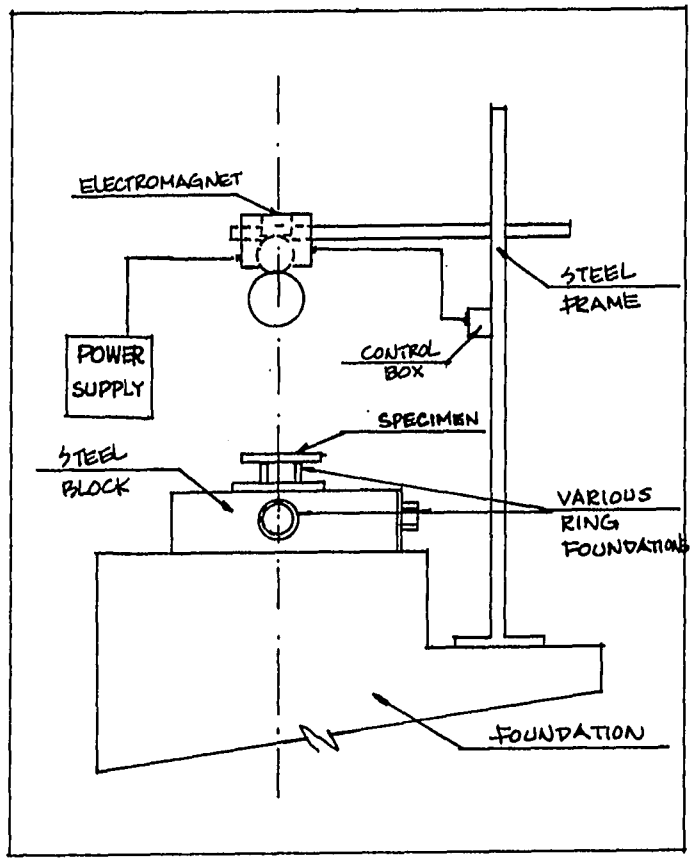

Fig. 15. Experimental set-up for impact loading

epoxy. The diameters of the ring foundation were 1/4", 1/2" and 1". The surfaces of the glass plate specimens (1/4" x 3" x 3") were cleaned with Acetone. An electromagnet was used for controlling the release of the steel ball onto the glass surface. The electromagnet was held in position by being partially contained in a box which was mounted on an adjustable stationary steel frame (Fig. 15). For the purpose of alignment, two small steel balls of diameter 1/4" were connected by an adjustable fine thread. One steel ball (1/4" dia) was held by the electromagnetic system just over the center of the ring foundation and the other steel ball (1/4" dia) was used to check the alignment of the center of the impact steel ball (1 $\frac{3}{4}$" dia) and the ring foundation by lowering the lower small ball down to the ring foundation. At specified heights of fall, several impacts were made until a crack occurred. The number of impacts required for fracture and the corresponding height of fall were recorded. From these data, the distribution curves for the probability of fracture were obtained as shown in Fig. 16.

B. Results

From the distribution curves plotted on the basis of the experimental data in Fig. 16, the heights of fall for 50% probability of fracture can be determined. From those heights, the corresponding velocities of impact can be calculated.

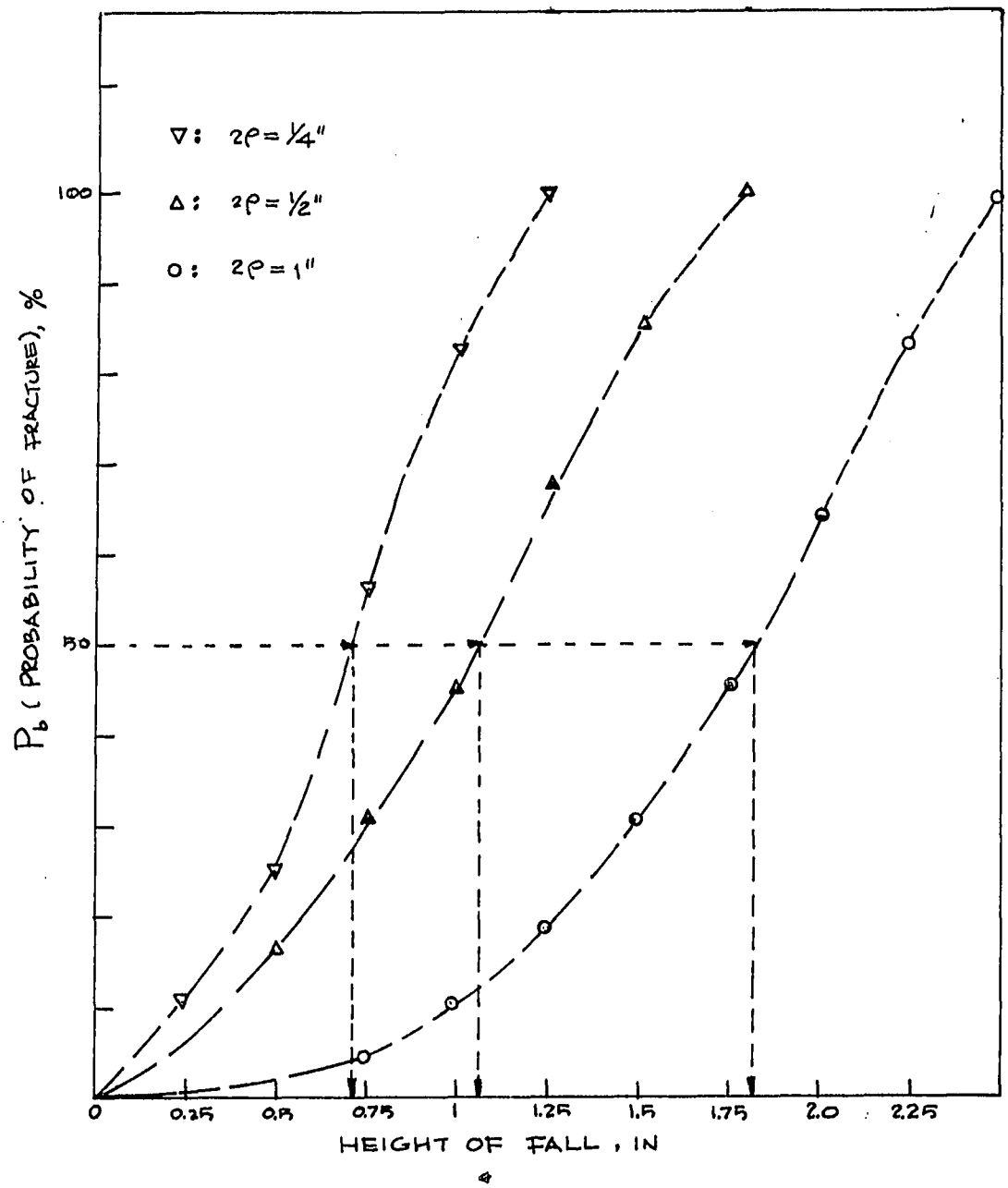

Fig. 16. Distribution curves for probability of fracture

These velocities are called the fracture velocities of impact and are plotted in Fig. 17 as a function of the diameter of the ring foundation. It can be seen that the fracture velocity increases with increasing support diameter or span. In other words, the impact energy required for fracture increases if the support span increases. For the foundation diameters of 1/4" and 1/2", Hertzian fractures or conic fractures were observed in the upper surfaces of the specimen. For the largest diameter of 1", flexure fractures were observed, which initiated from the center of the lower surface of the specimen and finally ruptured the whole specimen.

For the fracture impact velocities measured experimentally, two possible maximum tensile stresses are involved (35). The first one is the radial stress which occurs along the contact circle in the upper plate surface. The second possible critical stress is the circumferential stress which occurs at the point opposite the contact center in the lower plate surface. These two stresses were calculated using Equations C20, C22 and C24 in Appendix C for all the fracture impact velocities measured. The results are shown in Table 1. It was shown in (35) that the value of the critical tensile stress for Hertzian fracture was much higher than that for flexure fracture. As can be seen in Table 1, σ_{rr} for $\rho/H = 1$ and 2 and $\sigma_{\phi\phi}$ for $\rho/H = 4$ are comparable to, whereas the others are much lower than the corresponding critical stresses in (35). In other words, σ_{rr}

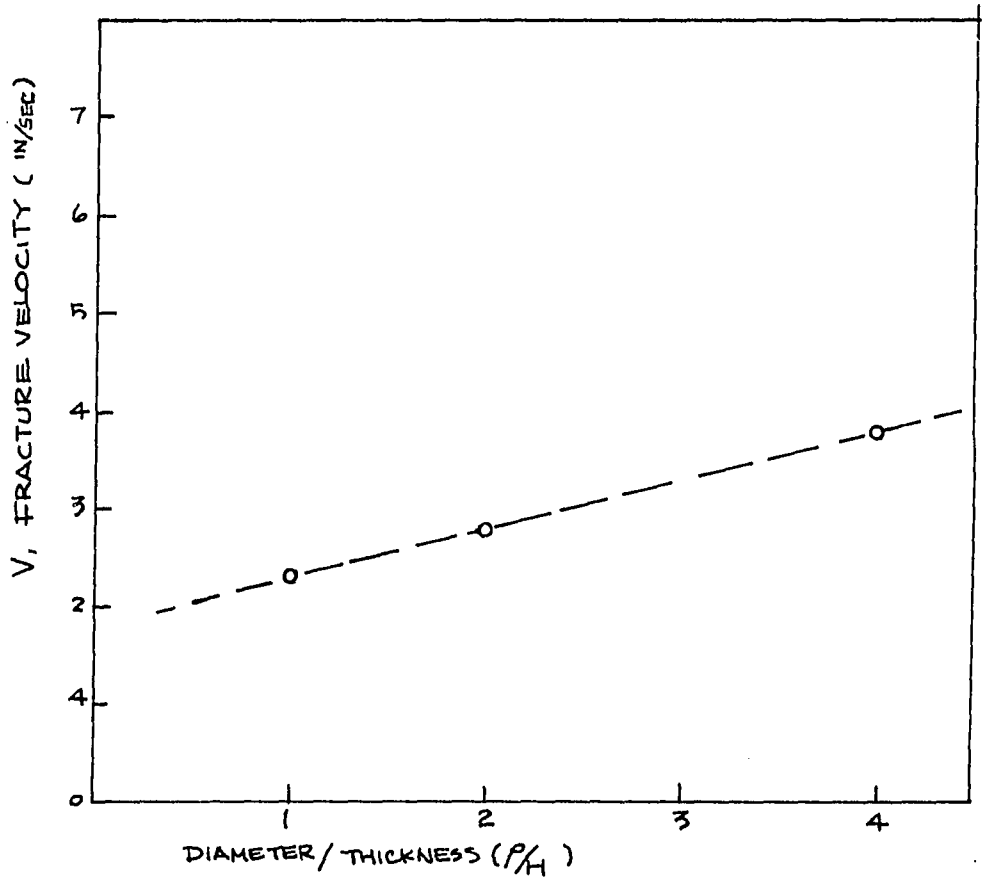

Fig. 17. Fracture velocity of impact

Table 1. Values of V, σ_{rr} and $\sigma_{\phi\phi}$ for $\rho/H = 1$ and 4

	Velocity (in./sec)	Stress σ_{rr} (lb/in.^{2})	Stress $\sigma_{\phi\phi}$ (lb/in.^{2})
$\rho/H = 1$	23.35	44,302	9,282
$\rho/H = 2$	28.67	37,648	15,502
$\rho/H = 4$	37.37	30,405	23,598

governed and thus Hertzian fracture was observed for $\rho/H = 1$ and 2. For $\rho/H = 4$, σ_{rr} became lower than its critical value whereas $\sigma_{\phi\phi}$ reached the corresponding critical value. Therefore, different type of fracture, flexure fracture, was observed.

VI. CONCLUSION AND SUMMARY

The low decelerating and accelerating speed of a flexure crack propagating in a specimen of glass plate was produced and measured experimentally. The specimen was supported on its lower surface by a knife-edged (Fig. 1a) or ring foundation (Fig. 1b) and subjected to a spherical indentation on its upper surface at the center of the foundation. The sizes of the specimens were 17.78 x 7.62 x 0.3175 cm. The specimen was loaded statically until a crack started to propagate. A single crack was propagated along the centerline of the specimen on the knife-edged support. For the ring support, however, mutually perpendicular double cracks were propagated, one being along the specimen centerline. The method of an electrically conductive grid was used to measure the crack speeds (Figs. 2a-2d), which range from 36 m/sec to 476 m/sec along the specimen centerline. The speeds are small compared to the limiting speed of 1500 m/sec (1). In the range of the speeds measured, the inertia effects were shown to be small (41) and are neglected in the present analysis. Since the spans of the foundations used were comparable to the specimen thickness, three-dimensional stress fields were established in the specimens under loading. The description of the three-dimensional stress distribution in the pre-fracture state was presented in terms of the stretching and bending stress components using

Love's strain functions (36). It was shown that the variation of the crack speed does not depend on the total surface tensile stress, but depends on the in-plane averaged stretching stress. The averaged stretching stress was shown to be compressive in the region nearby the knife-edged supports where the crack speed was observed experimentally to be decreasing (Fig. 2a). Furthermore, the magnitudes of the stretching stresses produced in the experiments were determined to be small so that the low varying crack speed, instead of the high limiting speed (1), was measured experimentally.

Experimental measurements were also made on the speed of a flexure crack propagating in a PMMA plate specimen which was subjected to a loading similar to that for the above glass specimens. The crack speeds range from 1.3 m/sec to 13 m/sec, which is small compared to the limiting speed of 670 m/sec (39). They are also smaller than the corresponding values for the glass specimens. The value of the crack speeds measured is oscillating along the distance of propagation and increases at a low rate. The slowness and the low rate of increase of the flexure crack is shown as a result of the combined effect of the high surface energy of PMMA and the low in-plane stretching stress in the specimen.

The surface energy of PMMA plates under transverse static and dynamic loadings was measured experimentally. The MTS machine in the Department of Engineering Science and Mechanics,

Iowa State University, was employed in the measurement of the quasi-static surface energy. The value measured is 4.62×10^5 erg/cm^2 which is comparable to the values obtained from different experimental methods. A piezoelectric accelerometer was incorporated into an impact system which was designed, fabricated and used for measurement of the dynamic surface energy of PMMA plate. On the basis of the outputs obtained from the accelerometer, the dynamic surface energy was measured as 5.55×10^5 erg/cm^2 which is higher than its quasi-static value.

Dynamic fractures in glass plates were also investigated. A steel ball was made to impinge on the upper surface of a 1/4" thick glass plate specimen which was supported by a ring foundation on its lower surface. The ratio of the plate thickness to the radius of the ring foundation was chosen to be in the range where the transition from one type of fracture to the other type was observed experimentally. The first type observed was Hertzian fracture or conic fracture whereas the second type is flexure fracture. Conditions for the transition were suggested on the basis of the critical stresses calculated from an impact theory. The impact energy required for fracturing the specimens was measured experimentally to be increasing with increasing support radius.

VII. BIBLIOGRAPHY

1. H. Schardin, "Velocity Effects in Fracture," in Fracture, edited by B. L. Averbach et al. (John Wiley & Sons, New York, 1959), pp. 297-329.

2. N. Lundborg and C. H. Johanson, "Experimental Determination of the Speed of Propagation of Cracks in Glass as a Function of the Stress," Arkiv for Fysik 4, 555-558 (1952).

3. S. R. Bodner, "Stress Waves Due to Fracture of Glass in Bending," Journal of Mechanics and Physics of Solids 21, 1-8 (1973).

4. J. A. Kies, A. M. Sullivan and G. R. Irwin, J. Appl. Phys. 21, 716 (1950).

5. H. Kolsky, Stress Waves in Solids (Dover Press, New York, 1963).

6. D. L. Holt, J. Appl. Polym. Sci. 12, 1953 (1968).

7. B. Cotterell, Appl. Matls. Res. 4, 227 (1965).

8. S. R. Anthony, J. P. Chulb and J. Congleton, Philosophical Magazine 22, 1201-1216 (1970).

9. N. H. Watts and D. J. Burns, Polym. Eng. Sci., I, 90 (1967).

10. J. P. Berry, Nature, 185, 91 (1960).

11. I. Wolock and S. B. Newman, in Fracture Processes in Polymeric Solids, edited by B. Rosen (Interscience, New York, 1964), p. 235.

12. A. A. Griffith, Phil. Trans. Roy. Soc. A221, 163 (1920).

13. C. E. Inglis, Trans. Inst. Naval Arch. 55, 219 (1913).

14. E. Orowan, Welding J. Res. Suppl., 34, 1575 (1955).

15. G. R. Irwin, in Fracturing of Metals (Am. Soc. Metals, Cleveland, Ohio, 1948), p. 147.

16. J. P. Berry, J. Polymer Sci., A1, 993 (1963).

17. J. W. Obreimoff, "The Splitting Strength of Mica," Proc. Roy. Soc. (London), A127, 290-297 (1930).

18. J. J. Gilman, "Direct Measurements of the Surface Energies of Crystals," J. Appl. Phys. 31, 2208-18 (1960).

19. W. F. Brace and J. B. Walsh, "Some Direct Measurements of the Surface Energy of Quartz and Orthoclase," The American Mineralogist 47, 1111-22 (1962).

20. A. R. C. Westwood and T. T. Hitch, "Surface Energy of (100) Potassium Chloride," J. Appl. Phys. 34, 3085-89 (1963).

21. P. L. Gutshall and G. E. Gross, "Cleavage Surface Energy of NaCl and MgCl in Vacuum," J. Appl. Phys. 36, 2459-60 (1965).

22. W. G. Knauss, Appl. Mech. Rev. 26, 1 (1973).

23. R. P. Kambour, J. Polym. Sci., A-2, 4, 349 (1966).

24. J. P. Andrews, Roy. Phys. Soc. (London) 43, 18 (1931).

25. J. P. A. Tillet, Proc. Phys. Soc. B69, 981 (1956).

26. F. C. Roesler, Proc. Phys. Soc. B69, 981 (1956).

27. Y. M. Tsai and H. Kolsky, J. Mech. Phys. Solids 15, 263 (1967).

28. G. P. Cherepanov and V. B. Sokolinsky, Eng. Fract. Mech. 4, 205 (1972).

29. B. R. Lawn and M. V. Swain, J. Mat. Sci. 10, 113 (1975).

30. M. V. Swain and J. T. Hagan, J. Phys. D. Appl. Phys. 9, 2201 (1976).

31. E. H. Lee and J. R. M. Rodak, "The Contact Problem for Viscoelastic Bodies," Journal of Applied Mechanics, 27, No. 3, 438-444 (Sept. 1960).

32. S. C. Hunter, "The Hertz Problem for a Rigid Spherical Indenter and a Viscoelastic Half Space," Journal of the Mechanics and Physics of Solids 8, 219 (1960).

33. P. I. Vincent, Impact Tests and Service Performance of Thermoplastics, Plastic Institute, London (1971).

34. C. B. Buchnall, K. V. Gotham, P. I. Vincent in Polymer Science, edited by A. D. Jenkins (North-Holland Publ., Amsterdam, The Netherlands, 1972), Chapt. 10.

35. Y. M. Tsai, "Stress Distributions and Fracture Produced by a Spherical Indenter in a Glass Plate Resting on a Ring Foundation," Midwest Mechanics Conference Proceedings 11, 795-808 (1969).

36. Y. C. Fung, Foundations of Solid Mechanics (Prentice-Hall, Englewood Cliffs, New Jersey, 1965).

37. I. N. Sneddon, Fourier Transforms (McGraw-Hill, New York, 1951).

38. Y. M. Tsai, "Stress Distributions in Elastic and Visco-elastic Plates Subjected to Symmetrical Rigid Indentations," Quarterly of Applied Mathematics 27, 371-380 (1968).

39. K. Katsamanis, D. Raftopuloe and P. S. Theocaris, "The Dependence of Crack Velocity on the Critical Stress in Fracture," Experimental Mechanics 17, 128-132 (April 1977).

40. R. N. Harward, The Physics of Glassy Polymers (Wiley, New York, 1973).

41. Y. M. Tsai, "Propagation of a Brittle Crack at Constant and Accelerating Speeds," International Journal of Solids and Structures 9, 625-642 (1973).

VIII. ACKNOWLEDGEMENTS

The author expresses his sincere appreciation to Professor Y. M. Tsai for guidance and advice during his graduate career. He also wishes to express his appreciation for the financial support provided with the kind approval of Professor H. J. Weiss by the Engineering Research Institute at Iowa State University, partially through the National Science Foundation Grant No. ENG 74-08147. Equipment purchases and use were also obtained through Iowa State's Engineering Research Institute.

Particular thanks are due to my wife, Lin-Mei, for helping in many ways.

IX. APPENDIX A. CALCULATION OF a, V, δ AND f

In order to determine the surface energy of PMMA plate due to impact loading in Appendix B, experimental data are prepared and details of preparation and calculation are presented in the following two cases.

A. Case 1 - Unfractured PMMA Plate

The photograph in Fig. 12 obtained from the impact experiments for the unfractured PMMA plate was converted as described on page 50 and is shown in Figs. 18 and 19 for the purpose of calculations. Experimental data obtained from the photograph and the related quantities are listed and defined as follows:

2ρ(diameter of ring foundation) = 1"

d (impact distance) = 16"

V_o(initial velocity) = 43.39 in./sec

a_p(peak acceleration) = 26,707 in./sec^2

f_p(peak force) = 55 lb

V:velocity (in./sec)

a:acceleration (in./sec^2)

f:force (lb)

δ:deflection (in)

t:duration time (sec)

W:work (lb-in.)

∂:surface energy (erg/cm^2)

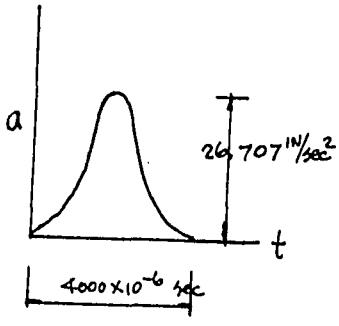

Fig. 18. Acceleration vs. duration time

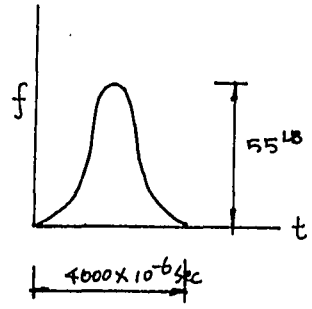

Fig. 19. Force vs. duration time

The main part of the curve in Fig. 12a is assumed to be a half sine curve and the acceleration of the steel ball can be written as:

$$a = -26{,}707 \sin\left(\frac{\pi t}{4000 \times 10^{-6}}\right), \quad 0 < t < 4000 \times 10^{-6} \text{ sec} \qquad \text{(A1)}$$

$$V = 26{,}707 \times \left(\frac{4000 \times 10^{-6}}{\pi}\right) \cos\left(\frac{\pi t}{4000 \times 10^{-6}}\right) + k_1 \qquad \text{(A2)}$$

At $t = 0$, $V = 43.39$ in./sec, $\therefore k_1 = 9.39$ in./sec.

Equation A2 can now be written as:

$$V = 26{,}707 \times \left(\frac{4000 \times 10^{-6}}{\pi}\right) \cos\left(\frac{\pi t}{4000 \times 10^{-6}}\right) + 9.39 \qquad \text{(A3)}$$

Again integrating Equation A3, the deflection curve is

$$\delta = 26{,}707 \times \left(\frac{4000 \times 10^{-6}}{\pi}\right)^2 \sin\left(\frac{\pi t}{4000 \times 10^{-6}}\right) + 9.39\ t + k_2 \tag{A4}$$

At $t = 0$, $\delta = 0$ $\therefore k_2 = 0$

Therefore, the deflection curve can be written as:

$$\delta = 26{,}707 \times \left(\frac{4000 \times 10^{-6}}{\pi}\right)^2 \sin\left(\frac{\pi t}{4000 \times 10^{-6}}\right) + 9.39\ t \tag{A5}$$

At various instants, the velocity, deflection and impact force are obtained and listed as

$t = 1600 \times 10^{-6}$ sec, $V = 19.9$ in./sec, $\delta = 0.0562$ in., $f = 52.34$ lb

$t = 2000 \times 10^{-6}$ sec, $V = 9.39$ in./sec, $\delta = 0.0621$ in., $f = 55$ lb

$t = 2356.2 \times 10^{-6}$ sec, $V = 0$ $\delta = 0.0637$ in., $f = 52.9$ lb

$t = 2800 \times 10^{-6}$ sec, $V = -10.6$ in./sec $\delta = 0.0613$ in., $f = 44.52$ lb

$t = 3550 \times 10^{-6}$ sec, $V = -22.51$ in./sec, $\delta = 0.0483$ in., $f = 19.05$ lb

$t = 4000 \times 10^{-6}$ sec, $V = -24.62$ in./sec, $\delta = 0.0376$ in., $f = 0$

B. Case 2 - Fractured PMMA Plate

The photograph in Fig. 12b obtained from the impact experiments for the fractured PMMA plate was converted as described on page 50 and is shown in Figs. 20 and 21 for the purpose of calculation. The quantities involved and obtained are as follows:

2ρ (diameter of ring foundation) = 1"

d (impact distance) = 16"

V_o (initial velocity) = 43.39 in./sec

a_p (peak accelerations) = 16,479 in./sec^2, 14,206 in./sec^2 and 18,184 in./sec^2

f_p (peak forces) = 33.96 lb, 29.27 lb and 37.47 lb

The initial parts of Figs. 20 and 21 are considered triangular whereas the later parts are assumed as parts of a half sine curve.

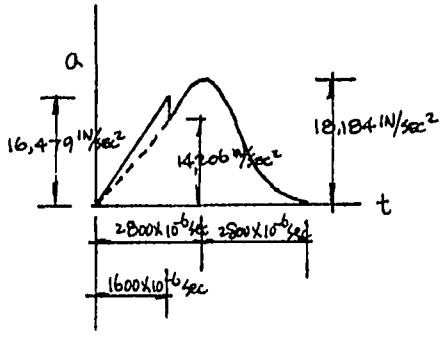

Fig. 20. Acceleration vs. duration time

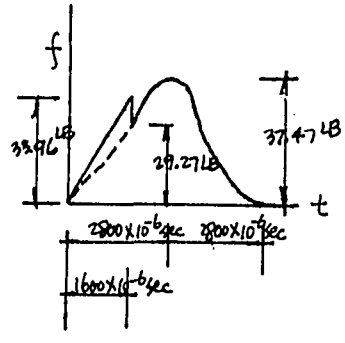

Fig. 21. Force vs. duration time

The initial acceleration curve can now be written as

$$a = - \frac{16479\ t}{1600 \times 10^{-6}} \quad , \ 0 < t < 1600 \times 10^{-6} \text{ sec} \tag{A6}$$

By integrating Equation A6, the velocity curve is

$$V = - \frac{16479\ t^2}{3200 \times 10^{-6}} + k_1 \tag{A7}$$

At $t = 0$, $V = 43.39$ in./sec, $\therefore k_1 = 43.39$ in./sec

$$\therefore V = \frac{-16479\ t^2}{3200 \times 10^{-6}} + 43.39 \tag{A8}$$

Again by integrating Equation A8 the deflection curve is

$$\delta = \frac{-16479\ t^3}{9600 \times 10^{-6}} + 43.39\ t + k_2 \tag{A9}$$

At $t = 0$, $\delta = 0$ $\therefore k_2 = 0$

$$\therefore \delta = \frac{-16479\ t^3}{9600 \times 10^{-6}} + 43.39\ t \tag{A10}$$

Values at various instants are

$t = 800 \times 10^{-6}$ sec, $V = 40.09$ in./sec, $\delta = 0.0338$ in.

$t = 1600 \times 10^{-6}$ sec, $V = 30.21$ in./sec, $\delta = 0.0624$ in.

The later part of the acceleration curve can be written as

$$a = -18184\sin\left(\frac{\pi t}{5600 \times 10^{-6}}\right), \quad 1600 \times 10^{-6}\text{sec} < t < 5600 \times 10^{-6}\text{sec} \tag{A11}$$

By integrating Equation A11 the velocity curve is

$$V = 18184\left(\frac{5600 \times 10^{-6}}{\pi}\right)\cos\left(\frac{\pi t}{5600 \times 10^{-6}}\right) + k_3 \tag{A12}$$

At $t = 1600 \times 10^{-6}$ sec, $V = 30.21$ in./sec,

$$\therefore k_3 = -2.2 \text{ in./sec}$$

$$\therefore V = 18184\left(\frac{5600 \times 10^{-6}}{\pi}\right)\cos\left(\frac{\pi t}{5600 \times 10^{-6}}\right) - 2.2 \tag{A13}$$

Again by integrating Equation A13, the deflection curve is

$$\delta = 18184\left(\frac{5600 \times 10^{-6}}{\pi}\right)\sin\left(\frac{\pi t}{5600 \times 10^{-6}}\right) - 2.2\ t + k_4 \tag{A14}$$

At $t = 1600 \times 10^{-6}$ sec, $\delta = 0.0624$ in. $\therefore k_4 = 0.02075$ in.

$$\therefore \delta = 18184\left(\frac{5600 \times 10^{-6}}{\pi}\right)^2\sin\left(\frac{\pi t}{5600 \times 10^{-6}}\right) - 2.2\ t + 0.02075 \tag{A15}$$

Values at various instants are

$t = 2000 \times 10^{-6}$ sec, $V = 11.86$ in./sec, $\delta = 0.0684$ in., $f = 33.76$lb

$t = 2356.2 \times 10^{-6}$ sec, $V = 5.79$ in./sec, $\delta = 0.0716$ in., $f = 36.32$lb

$t = 2678.9 \times 10^{-6}$ sec, $V = 0$ $\delta = 0.0725$ in., $f = 37.79$lb

$t = 2800 \times 10^{-6}$ sec, $V = -2.2$ in./sec, $\delta = 0.0724$ in., $f = 37.47$lb

$t = 3500 \times 10^{-6}$ sec, $V = -15.44$ in./sec, $\delta = 0.0657$ in., $f = 34.2$lb

$t = 4000 \times 10^{-6}$ sec, $V = -22.4$ in./sec, $\delta = 0.0571$ in., $f = 29.3$lb

$t = 5600 \times 10^{-6}$ sec, $V = -34.61$ in./sec, $\delta = 0.00843$ in., $f = 0$

X. APPENDIX B. CALCULATION OF SURFACE ENERGY

Surface energy is determined for both quasi-static and impact loadings. Details of calculations are as follows.

A. Case 1 - Quasi-Static Loading

By using the MTS machine, the data for the circular PMMA plate (4" diameter, 1'16" thick) resting on the ring foundation (1" diameter) (see Fig. 22) are obtained as follows:

P (the load just to fracture the specimen) = 42.5 lb

δ (the maximum deflection just at the initiation of crack) = 0.0197"

C (total crack length of the specimen after release of load) = 1.25"

h (thickness of specimen) = 1/16"

γ (surface energy, erg/cm^2)

According to the energy method, the relation is

$$\frac{P\delta}{2} = (2\gamma)hC \qquad (B1)$$

$$\gamma = 2.6792 \text{ lb}\cdot\text{in./in.}^2 = 4.62 \times 10^5 \text{ erg/cm}^2$$

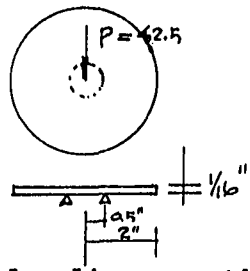

Fig. 22. A quasi-static loading on the circular PMMA plate resting on the ring foundation

B. Case 2 - Impact Loading

By using the steel ball (diameter 1 $\frac{3}{4}$") with accelerometer (the Columbia Model 902) to impinge onto the circular PMMA plate (4" diameter, 1/16" thick) which vertically rested on the ring foundation (1" diameter), the data for fracture energy are obtained (see Appendix A) as follows:

W_{max} (fractured energy obtained at t = 2000 x 10^{-6} sec)

$$= \frac{55 \times 0.0621 - 33.76 \times 0.0684}{2}$$

$$= 0.553 \text{ lb-in.}$$

C_D (total crack length of the specimen after one time impact) = 1.375"

$P_1 = 55$ lb, $\delta_1 = 0.0621$ in.

$P_2 = 33.76$ lb, $\delta_2 = 0.0684$ in.

h = (thickness of specimen) = 1/16"

γ_D = (surface energy, erg/cm^2)

According to the energy method, the relation is

$$\frac{P_1\delta_1}{2} - \frac{P_2\delta_2}{2} = W_{max} = (2\gamma_D)hC_D \qquad \text{(B2)}$$

By substituting the given data into Equation B2, the surface energy is

$$\gamma_D = 3.2175 \text{ lb in/in}^2 = 5.55 \times 10^5 \text{ erg/cm}^2$$

XI. APPENDIX C. DESCRIPTION OF IMPACT THEORY

An impact theory is to be developed to account for the experimental results presented in Sec. V-B. The contact time involved in the impact experiments is estimated to be around 300 μ sec. Therefore, it is assumed that the stresses and strains inside the ring support may be computed at any instant as though the contact were static. The assumption is similar to that used in the Hertz impact theory. Under this assumption, the total absolute normal displacement at the center of the contact area between the projectile and the plate can be obtained from (35). In view of the formulation of (35) and on the basis of the transformation u = 2HS, the absolute normal displacement at the contact center can be written as

$$\omega = u_z(\rho,H) - u_z(0,H) = \omega_H k_\omega(a/H,\ \rho/H) \tag{C1}$$

where

$$\omega_H = a^2/R \tag{C2}$$

$$k_\omega = 1 - \frac{1}{\pi}\frac{a}{H}\int_0^\infty \{\bar{\sigma}^I[B_I \cos\left(\frac{ua}{2H}\right) + B_{IV}]$$

$$- [B_{II} \cos\left(\frac{ua}{2H}\right) - B_{III} - B_V]\ \bar{\sigma}^{II}\}\ du \tag{C3}$$

$$B_I = (1 + u - e^{-u})/(\sinh u + u) \tag{C4}$$

$$B_{II} = (1 + u + e^{-u})/(\sinh u - u) \tag{C5}$$

$$B_{III} = [u\sinh u/2 + 4(1-\nu)\cosh u/2]/ [(\sinh u - u)2(1-\nu)] \tag{C6}$$

$$B_{IV} = 2\sinh^2 u/2\, J_o(u\rho/2H)/(\sinh u + u) \tag{C7}$$

$$B_V = 2[\cosh^2 u/2\, J_o(u\rho/2H) - \cosh u/2] - (u/2)\sinh(u/2)/(1-\nu) \tag{C8}$$

$$\bar{\sigma}^I = \int_0^1 k_p(x, \frac{a}{H}, \frac{\rho}{H}) \times [J_o\left(\frac{aux}{2H}\right) + J_o\left(\frac{u\rho}{2H}\right)]dx \tag{C9}$$

and

$$\bar{\sigma}^{II} = \int_0^1 k_p(x, \frac{a}{H}, \frac{\rho}{H}) \times [J_o\left(\frac{aux}{2H}\right) - J_o\left(\frac{\rho u}{2H}\right)]dx \tag{C10}$$

In the above expressions, a is the radius of contact, ν Poisson's ratio, R the radius of the spherical projectile, 2H the plate thickness and $J_o(x)$ the zeroth order Bessel function. Furthermore, k_p is the nondimensional function which was used to define the normal contact stress as follows (35):

$$p(r, \frac{a}{H}, \frac{\rho}{H}) = -(4a/C\pi R)\, k_p(x, \frac{a}{H}, \frac{\rho}{H}) \tag{C11}$$

where $C = (1-\nu)/\mu$, μ being the shear modulus of the material. Integration of Equation C11 gives the total contact force which was written (35) as:

$$P = -(8\ a^3/3\ CR)k_p(a/H,\ \rho/H) \tag{C12}$$

In terms of the total absolute normal displacement ω and the total contact force, Newton's equation of motion for the projectile of mass m can be written as:

$$m\ddot{\omega} = -P \tag{C13}$$

where dot denotes differentiation with respect to time. The above equation can be integrated to obtain a relationship between the impact velocity and the stress components in the plate. For the purpose of integration, ω in Equation C1 is differentiated with respect to a and the derivation is written as:

$$\frac{\partial \omega}{\partial a} = \omega_H' k_{\omega'}(a/H,\ \rho/H) \tag{C14}$$

where

$$\omega_H' = 2a/R \tag{C15}$$

and

$$k_{\omega'} = 1 + \frac{1}{\pi}\left(\frac{a}{2H}\right)^2 \int_0^\infty (B_I\bar{\sigma}^I - B_{II}\bar{\sigma}^{II})u \sin\left(\frac{ua}{2H}\right)du$$

$$- \frac{u}{2\pi a}\int_0^\infty \{[B_I\cos\left(\frac{ua}{2H}\right) + B_{IV}]\partial[\left(\frac{a}{H}\right)^3\bar{\sigma}^I]/\partial\left(\frac{a}{H}\right)$$

$$-[B_{II}\cos\left(\frac{ua}{2H}\right) - B_{III} - B_V]\partial[\left(\frac{a}{H}\right)^3\bar{\sigma}^{II}]\partial\left(\frac{a}{H}\right)\}du \qquad (C16)$$

Equation C13 can be integrated if it is multiplied by $\dot{\omega}$. The integration in terms of Equations C12 and C14 gives

$$\frac{m}{2}(\dot{\omega}^2 - V^2) = -\frac{16a^5}{15CR^2} - \int_0^a P_H\omega_H'[k_p k_{\omega'} - 1]da \qquad (C17)$$

where V is the initial velocity of impact of the sphere. If the transformation y = a/H is introduced, Equation C17 can be written as

$$\frac{m}{2}(\dot{\omega}^2 - V^2) = -\frac{16a^5}{15CR^2}\, k_v^2\,(\frac{a}{H}, \frac{\rho}{H}) \qquad (C18)$$

where the nondimensional function is

$$k_v^2 = 1 + 5(\frac{H}{a})^5 \int_0^{a/H} y^4[k_p(y,\rho/H)k_{,}(y,\rho/H) - 1]dy \qquad (C19)$$

When the impact reaches its maximum compression with the maximum contact radius of a_1, the velocity of the sphere vanishes, i.e., $\dot{\omega} = 0$.

Under this condition, the square root of the reduced equation of Equation C18 can be written as

$$V = V_H k_V \left(\frac{a_1}{H}, \frac{\rho}{H} \right) \tag{C20}$$

where the associated impact velocity is

$$V_H = (32\ a_1^5/15CR^2m)^{1/2} \tag{C21}$$

The nondimensional functional values of k_v in Equation C20 were calculated by using an electronic computer and its value is shown in Fig. C1 as a function of the nondimensional parameters a/H and ρ/H, a_1 being replaced by a for convenience in notation and application. For a given set of V, R, H, and ρ, the maximum contact radius a_1 can be determined from Equation C20 by a trial-and-error method similar to that used in (35). Once a_1 has been calculated, the stresses concerned can be calculated as described in (35). The stresses which are of importance for the two experiments concerned are the following two possible maximum tensile stresses. The first maximum tensile stress is the radial stress along the contact circle:

$$\sigma_{rr}(a,H,\rho) = {}_H\sigma_{rr}(a) k_\sigma^+ [\nu,\ a/H, \rho/H] \tag{C22}$$

where the associated half-space tensile stress is

$$_{H}\sigma_{rr}(a) = -(1 - 2\nu)P_H/2\pi a^2 \qquad \text{(C23)}$$

The second possible maximum tensile stress is the circumferential stress which occurs at the center of the lower surface as follows:

$$\sigma_{\phi\phi}(0,-H,\rho) = {}_{H}\sigma_{rr}(a)k_{\sigma}^{-}(\nu,a/H,\rho/H) \qquad \text{(C24)}$$

The curves for the nondimensional functions k_{σ}^{+} and k_{σ}^{-} were both determined and given in (35).

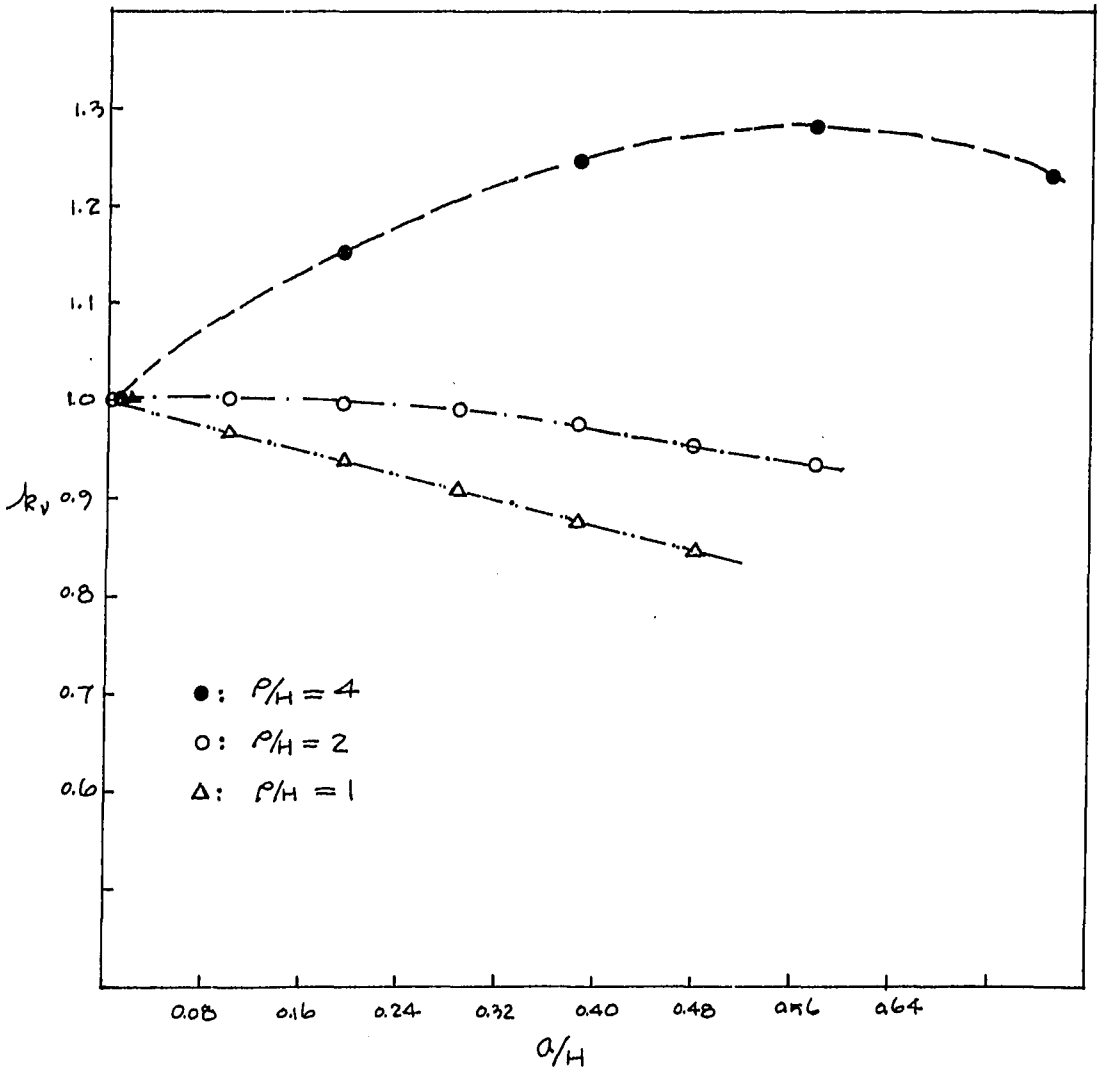

Fig. C1. Curves of k_v vs. a/H for ρ/H = 1, 2 and 4